

# Scaling crossover of the generalized Jeffreys-type law\*

Fugui Ma <sup>†</sup>

**Abstract.** The generalized Jeffreys-type law is formulated as a multi-term time-fractional Jeffreys-type equation, whose dynamics exhibit rich scaling crossover phenomena entailing different diffusion mechanisms. In this work, we provide a novel physical explanation for the equation from first principles, beginning with a microscopic description based on the continuous-time random walk framework with a generalized waiting time distribution and further deriving the equation from an overdamped Langevin equation subject to a stochastic time-change (subordination). Employing the Laplace transform method, we conduct a rigorous analysis of the equation, establishing its well-posedness and providing a detailed Sobolev regularity analysis. We also develop a novel numerical scheme, termed the CIM-CLG algorithm, which achieves spectral accuracy in both time and space while substantially relaxing the temporal regularity requirements on the solution. The algorithm reduces the computational complexity to  $\mathcal{O}(N)$  in time and  $\mathcal{O}(M \log M)$  in space and is fully parallelizable. Detailed implementation guidelines and new technical error estimates are provided. Extensive numerical experiments in 1D and 2D settings validate the efficiency, robustness, and accuracy of the proposed method. By integrating stochastic modeling, mathematical analysis, and numerical computation, this work advances the understanding of the generalized Jeffreys-type law and offers a mathematically rigorous and computationally efficient framework for tackling complex nonlocal problems.

**Key words.** Jeffreys-type law, CTRW, Langevin equation, regularity, contour integral method, Chebyshev-Legendre Galerkin spectral method

**MSC codes.** 60K50, 65M12, 65M70, 65E10, 82C31

## 1. Introduction.

**1.1. Macro phenomenological Jeffreys-Type law.** Diffusion refers to the net movement of particles or molecules from a region of high concentration to one of lower concentration, driven by a concentration gradient [18]. This process was first formulated mathematically by Adolf Fick in 1855 [24, 25], and is now known as Fick's law of diffusion. Fick's first law describes steady-state diffusion at the macroscopic level, stating that the diffusion flux  $J(t, r)$  (defined as the amount of substance per unit area per unit time, in  $[mol/(m^2 \cdot s)]$ ) is proportional to the negative gradient of the concentration  $\nabla \varphi(t, r)$ , where  $\varphi(t, r)$  denotes the concentration (in  $[mol/m^3]$ ). This relationship is expressed as  $J(t, r) = -D_1 \nabla \varphi(t, r)$ , where  $D_1$  is the diffusion coefficient (in  $[m^2/s]$ ) [16]. When the concentration profile changes over time, the system is no longer in a steady state, and Fick's second law must be applied. By combining the continuity equation,  $\partial_t \varphi(t, r) + \text{div } J(t, r) = 0$  (see, e.g., [30, Eq. (1.3)]), with Fick's first law, one derives Fick's second law, i.e.,  $\partial_t \varphi(t, r) - D_1 \Delta \varphi(t, r) = 0$  [33]. It seems widely accepted that Fick's law of diffusion was developed by analogy with Fourier's law of heat conduction, which leads to a mathematically identical equation known as the heat equation or the law of thermal conductivity [18, 27], albeit with different physical interpretations of

\*Submitted to the editors DATE.

**Funding:** This work was funded by the Peking University Boya postdoctoral fellowship.

<sup>†</sup>School of Mathematical Sciences, Peking University, Beijing, 100871, China ([mafugui@math.pku.edu.cn](mailto:mafugui@math.pku.edu.cn)).

the variables. In practice, however, diffusion processes are often influenced by factors such as temperature, concentration gradients, particle size, and properties of the medium, leading to different diffusion types. Diffusion that conforms to Fick's laws is termed normal diffusion (ND) or Fickian diffusion, while diffusion that deviates from these laws is referred to as anomalous diffusion (AD) or non-Fickian diffusion [52].

Fick's law of diffusion is widely employed in transport theory [33], yet it does not account for the inertia of the diffusing particles or molecules [30]. As a result, the classical diffusion equation provides an accurate description only in weakly inhomogeneous media or under slow processes where the relaxation time is longer than the characteristic time scale [57]. In other scenarios, this model may prove inadequate. This limitation has motivated numerous modifications of Fick's law to better represent mass transfer dynamics (see, e.g., [2, 12, 30]).

The simplest modification of Fick's law that accounts for inertial effects in moving particles is Cattaneo's equation (CE),  $\tau\partial_t J(t, r) + J(t, r) = -D_2\nabla\varphi(t, r)$ , where  $\tau$  denotes the relaxation time [30]. This constitutive law extends Fick's first law by introducing a correction term proportional to the time derivative of the diffusion flux,  $\partial_t J(t, r)$ . The presence of this term reflects that the flux  $J(t, r)$  takes a finite relaxation time  $\tau$  to become established, rather than responding instantaneously. Combining Fick's law and CE yields a more general constitutive relation

$$(1.1) \quad \tau\partial_t J(t, r) + J(t, r) = -\chi(1 + \tau_2\partial_t)\nabla\varphi(t, r), \quad \forall t > 0,$$

where  $D_1 > 0$ ,  $\chi := (D_1 + D_2)/2 > 0$ , and  $\tau_2 = \tau D_1/(D_1 + D_2)$  is an additional relaxation time. The constitutive relation (1.1) is referred to as the Jeffreys-type law [7, 30, 57]. Notably, as  $\tau \rightarrow 0$ , equation (1.1) reduces to Fick's law, and when  $D_1 = 0$ , it simplifies to Cattaneo's equation. Solving (1.1) yields the flux expression  $J(t, r) = -D_1\nabla\varphi(t, r) - \frac{D_2}{\tau} \int_0^t e^{-(t-s)/\tau} \nabla\varphi(s, r) ds + e^{-t/\tau} (D_1\nabla\varphi_0 + J_0)$  with initial conditions  $\varphi_0 = \varphi(0, r)$  and  $J_0 = J(0, r)$  representing the distribution of concentration and flux at  $t = 0$  [30], respectively. Substituting this result into the continuity equation and eliminating  $J(t, r)$  leads to the Jeffreys-type equation (JE) [7]

$$(1.2) \quad \partial_t\varphi(t, r) + \tau\partial_t^2\varphi(t, r) = \chi(1 + \tau_2\partial_t)\Delta\varphi(t, r), \quad \forall t > 0,$$

where  $r \in \mathbb{R}^n$  ( $n = 1, 2, 3$ ). When  $\tau = 0$ , (1.2) reduces to Fick's second law; when  $D_1 = 0$  (implying  $\tau_2 = 0$ ), it becomes the telegrapher's equation (TE). The TE is a hyperbolic equation that represents the simplest model integrating damped thermal waves alongside parabolic diffusion [48, 58], and serves as a fundamental link between circuit theory and electromagnetic field theory.

Although the Jeffreys-type law provides an important and intuitive modification to Fick's law, it remains essentially a phenomenological model that lacks rigorous derivation from first principles, and thus suffers from limited physical interpretability. In this work, we conduct a comprehensive study of a class of generalized Jeffreys-type laws, which constitute a well-established extension of both Fourier's law and Fick's law in the context of heat and mass transport. Unlike previous macroscopic derivations of diffusion equations or the JE, our approach rigorously derives the generalised Jeffreys-type law from microscopic particle transport dynamics. This foundation derivation not only provides a clearer physical interpretation but also enables a multi-faceted exploration of the law through perspectives such as stochastic modeling, PDE analysis, and numerical analysis.

**1.2. Micro stochastic modeling: Scaling crossover.** At the microscopic level, the ND corresponds to Brownian motion, characterized by a consistent random-walk picture of diffusing particles [65] and aligning with a Markovian stochastic process [52]. This indicates that the distribution function remains Gaussian for all times [2]. Let  $X(t)$  be a stochastic process, the mean-squared displacement (MSD) is defined as the ensemble average  $\langle X^2(t) \rangle := \int_{-\infty}^{\infty} r^2 p(t, r) dr$  with  $p(t, r)$  being the probability density function (PDF) of finding a particle at position  $r$  at time  $t$ . It is observed that Brownian motion exhibits the scaling  $\langle X^2(t) \rangle \sim t$  (for further discussion, see [65]). While the AD exhibits an MSD that may follow a scaling relation  $\langle X^2(t) \rangle \sim t^\alpha$  with  $\alpha \neq 1$ . Based on the scaling exponent  $\alpha$ , the process is classified as follows: when  $0 < \alpha < 1$ , it is termed subdiffusion; when  $1 < \alpha < 2$ , it is referred to as superdiffusion; when  $\alpha = 2$ , it is known as ballistic diffusion [6, 52]. In recent years, a growing body of research has focused on AD, as reflected in works such as [10, 11, 19, 31, 52].

Recent experimental studies have demonstrated that the diffusion of microscopic active particles often exhibits scaling crossover, characterized by a transition between different diffusion regimes over time (e.g., from short-time superdiffusion to long-time normal diffusion). We term this phenomenon crossover diffusion (CD), marked by the scaling exponent  $\alpha$ . Such behavior has been observed in diverse systems, including: molecular diffusion during polymerization-depolymerization, transitioning from subdiffusion to normal diffusion [66]; self-propelled colloids in quasi-2D suspensions, showing a rapid crossover from subdiffusion to normal diffusion [56]; fermion-fermion scattering under weak interactions, exhibiting dynamical features that crossover from early-time ballistic diffusion to late-time normal diffusion [37]; water molecules in the hydration shell of proteins, undergoing a transition from subdiffusion to normal diffusion [68]; and swimming bacteria described by Lévy walks, displaying a crossover from ballistic to normal diffusion [54].

In addition to experimental studies, researchers have begun to investigate crossover diffusion (CD) using microscopic stochastic models. Relevant contributions include, but are not limited to, the following: Masoliver [48] generalize the TE to model AD, obtaining a space-time fractional telegrapher's equation that captures two distinct dynamic regimes,  $\langle X^2(t) \rangle \sim t^{2\alpha}$  as  $t \rightarrow 0^+$  and  $\langle X^2(t) \rangle \sim t^\alpha$  as  $t \rightarrow +\infty$ . Specifically, this models leads to a retarded subdiffusion process for  $0 < \alpha < 1/2$  and a transition from superdiffusive to subdiffusive behavior for  $1/2 < \alpha < 1$ . E. Awad and R. Metzler [6] examined generalized Cattaneo-type equations and demonstrated their capacity to transition from superdiffusion to subdiffusion. Ma et al. [43] studied a time-fractional normal-subdiffusion transport equation, illustrating the crossover in MSD from ND to subdiffusion. Notably, E. Awad et al. [5] extended the JE to derive the time fractional Jeffreys-type equation (TFJE)

$$(1.3) \quad (1 + a {}_0^{RL} \mathfrak{D}_t^\alpha) \partial_t p(t, r) = k {}_0^{RL} \mathfrak{D}_t^{1-\gamma} (1 + b {}_0^{RL} \mathfrak{D}_t^\beta) \Delta p(t, r), \quad \forall t > 0,$$

where  $0 < \alpha, \beta, \gamma < 1$ ,  $a, b > 0$ ,  $k > 0$ , and the Riemann-Liouville time fractional derivative  ${}_0^{RL} \mathfrak{D}_t^s$  is defined by  ${}_0^{RL} \mathfrak{D}_t^s u(t) := \frac{1}{\Gamma(1-s)} \frac{d}{dt} \int_0^t (t-\tau)^{-s} u(\tau) d\tau$  with  $1 > s > 0$ . In [7], the authors established a connection between the TFJE and microscopic stochastic process, showing that the MSD exhibits various anomalous behaviors such as retarded and accelerated subdiffusion, as well as a crossover from superdiffusion to subdiffusion. Subsequently, Bazhlekova [8] further

generalized the model to the multi-term time-fractional Jeffreys equation (MT-TFJE)

$$(1.4) \quad \left(1 + a_0^{RL} \mathfrak{D}_t^\alpha + \sum_{k=1}^K a_k {}_0^{RL} \mathfrak{D}_t^{\alpha_k}\right) \partial_t p(t, r) = {}_0^{RL} \mathfrak{D}_t^{1-\gamma} \left(1 + b_0^{RL} \mathfrak{D}_t^\beta + \sum_{j=1}^J b_j {}_0^{RL} \mathfrak{D}_t^{\beta_j}\right) \Delta p(t, r),$$

for all  $t > 0$ , with the parameter constraints

$$(1.5) \quad \begin{cases} 0 < \alpha_k < \alpha \leq 1, \ 0 < \beta_j < \beta \leq 1, \ 0 < \gamma \leq 1, \ a > 0, \ b > 0, \ a_k \geq 0, \ b_j \geq 0, \\ k = 1, 2, \dots, K, \ j = 1, 2, \dots, J, \ K, J \in \mathbb{N}_+. \end{cases}$$

In accordance with the nomenclature of Jeffreys-type law, we designate (1.4) as the generalized Jeffreys-type law. While this model represents a necessary preliminary step, it currently lacks a detailed physical justification, as well as rigorous mathematical analysis and numerical analysis in a bounded domain.

Admittedly, numerous studies have investigated multi-term time-fractional differential equations (MT-TFDEs), which were developed to improve the modeling accuracy of the single-term counterparts, as evidenced in works such as [13, 29, 41, 47, 64]. However, the present study on the generalized Jeffreys-type law (1.4) diverges from previous research on MT-TFDEs in several key aspects: (i) Structural difference: The MT-TFJE exhibits a fundamentally different form from typical MT-TFFDEs. Existing studies on MT-TFDEs typically involve multi-term fractional derivatives on only one side of the equation, lacking the composite operator structure present on the right-hand side of (1.4). (ii) Generality and reducibility: By choosing specific parameters, MT-TFJE can be reduced to a wide range of established equations, demonstrating that they constitute a more general framework than other MT-TFDEs. For instance, when  $b = b_j = 0$ , MT-TFJE reduces to MT-TFDE; when  $a_k = b_j = 0$ ,  $\alpha = \beta = \gamma = 1$ , MT-TFJE becomes the classical JE; when  $a = a_k = 0$ ,  $b = b_j = 0$ , it reverts to standard sub-diffusion equation; when  $a_k = b_j = 0$ , it corresponds to the time-fractional telegrapher's equation. The versatile structure of MT-TFJE and its ability to capture crossover diffusion, as noted in previous studies, motivate a thorough and detailed investigation of this equation.

**1.3. Problem setup and summary of contributions.** This paper is structured around a threefold analysis of the MT-TFJE, encompassing its stochastic modeling, the establishment of solution theory and regularity properties, and the development of a numerical method with spatio-temporal spectral accuracy. These efforts may advance the understanding of MT-TFJE and provide novel methodological insights to the field.

Firstly, we establish two types of stochastic models at the microscopic level, based on the continuous-time random walk (CTRW) framework and the overdamped Langevin equation, to provide a physical interpretation for the MT-TFJE. In Model *I*, an extended CTRW model is constructed using a generalized waiting time distribution combined with a Gaussian step size distribution. By evaluating the MSD, we analyze the asymptotic behavior of the stochastic process at the microscopic scale and investigate the rich crossover diffusion mechanisms described by the MT-TFJE. Building on the understanding gained from model *I*, we develop Model *II* by coupling the overdamped Langevin equation with a time-changing process, establishing a connection with the CTRW model and offering an alternative perspective on the microscopic physical interpretation of the MT-TFJE.

Secondly, we generalize the MT-TFJE by incorporating suitable initial and boundary conditions along with a suitably defined source term, which leads to the following well-posed problem:

$$(1.6) \quad \begin{cases} {}_0^{RL}\mathfrak{J}_t^{1-\gamma} \left( 1 + a {}_0^{RL}\mathfrak{D}_t^\alpha + \sum_{k=1}^K a_k {}_0^{RL}\mathfrak{D}_t^{\alpha_k} \right) \partial_t p(t, r) \\ \quad = - \left( 1 + b {}_0^{RL}\mathfrak{D}_t^\beta + \sum_{j=1}^J b_j {}_0^{RL}\mathfrak{D}_t^{\beta_j} \right) \mathcal{A}p(t, r) + f(t, r), \quad (t, r) \in (0, T] \times \Omega, \\ p(0, r) = p_0, \quad \lim_{t \rightarrow 0} \partial_t p(t, r) = 0, \quad (t, r) \in \{0\} \times \Omega, \\ p(t, r) = 0, \quad (t, r) \in (0, T] \times \partial\Omega, \end{cases}$$

where  $\Omega \subset \mathbb{R}^n$  ( $n = 1, 2, 3$ ) is a bounded convex polygonal domain with smooth boundary  $\partial\Omega$ , and  $T > 0$ . The parameters satisfy the constraints given in (1.5). Here,  ${}_0^{RL}\mathfrak{J}_t^s$  denotes the Riemann-Liouville fractional integral operator, defined for  $0 < s < 1$  by  ${}_0^{RL}\mathfrak{J}_t^s u(t) := \frac{1}{\Gamma(1-s)} \int_0^t (t-\tau)^{-s} u(\tau) d\tau$ , and  $\mathcal{A}$  is a second-order self-adjoint, closed, positive definite spatial operator. The source term belongs to the space  $f \in L^1(0, T; L^1(\Omega))$ .

Next, we analyze the well-posedness and regularity of the solution to Problem (1.6), establishing a solution theory within a rigorous mathematical framework. Existing studies on MT-TFDEs often rely on the Mittag-Leffler function to examine well-posedness and regularity (see, e.g., [8, 29, 41, 47, 64]). Different from such methods, our work employs the Laplace transform method, which offers the advantage of more directly connecting solution properties with the characteristic functions arising in stochastic modeling. This approach not only bridges stochastic models with analytical techniques but also establishes a clear connection between model construction and mathematical analysis.

Due to the complex form of the equation and the historical memory and non-local property inherent in multi-term time fractional differential operators, obtaining exact solution for MT-TFJE is often challenging. As a result, numerical methods are indispensable for solving such equation. Currently, the primary numerical methods for the temporal semi-discretization of MT-TFDEs fall into two categories: the  $L1$ -type scheme (see, e.g., [23, 29, 55]) and convolution quadrature (CQ) methods (see, e.g., [17, 20, 40]). A major limitation common to both methods is their substantial computational and memory requirements, with arithmetic complexities of  $\mathcal{O}(N^2)$  and  $\mathcal{O}(N)$ , respectively. Even in one-dimensional settings, when combined with spatial semi-discretization involving  $M$  degrees of freedom, the total computational cost increases to  $\mathcal{O}(N^2 M^2)$ , placing severe demands on computational resources. Moreover, these methods generally require a high solution regularity to maintain their theoretical convergence orders.

Finally, to overcome the limitations discussed above, we propose a novel numerical scheme that achieves spectral accuracy in both time and space while significantly relaxing temporal regularity requirements on the solution. Specifically, we extend the contour integral method (CIM) (see, e.g., [14, 34, 35, 39, 43, 44, 50, 67, 69]) to construct a semi-discrete scheme in time, which is then coupled with a Chebyshev-Legendre Galerkin (CLG) spatial semi-discrete scheme (see, e.g., [46, 61–63, 70, 71]) to form a fully discrete scheme, termed CIM-CLG algorithm. By incorporating fast Fourier transform (FFT) for acceleration, our approach reduces

the temporal computational cost to  $\mathcal{O}(N)$  with only  $\mathcal{O}(1)$  storage overhead, and the spatial cost to  $\mathcal{O}(M \log M)$ , leading to a substantial improvement in efficiency. Meanwhile, we provide a rigorous error analysis of the proposed scheme and demonstrate its high numerical efficiency, stability and robustness through numerical experiments in both one- and two-dimensional settings. Furthermore, the algorithm achieves spatio-temporal spectral accuracy, supports full (100%) parallelization, and requires low (or even no) temporal regularity requirements. This framework thus provides a computationally efficient and mathematically sound foundation for solving high-dimensional or long-time MT-TFDEs.

**1.4. Outline of paper.** The rest of the paper is organized as follows. In Section 2, the CTRW model with a generalized waiting-time distribution and an overdamped Langevin equation coupled with a time-changing stochastic process are used to derive the MT-TFJE from first principles, thereby providing a physical interpretation. Asymptotic analysis at different time scales is also performed to explore the rich crossover diffusion behaviors described by the model. In Section 3, we analyze the regularity of solution to the MT-TFJE. A priori estimates are established for both smooth and non-smooth initial data, and an improved regularity result is derived under certain conditions. In Section 4, we develop a novel numerical scheme, termed CIM-CLG, that achieves spatio-temporal spectral accuracy. Rigorous error estimates are provided, a strategy for determining the optimized parameters of a parameterised hyperbolic integral contour is proposed, and implementation details of the scheme are discussed. In Section 5, the effectiveness and robustness of the spatio-temporally spectral accuracy CIM-CLG are demonstrated via several numerical examples in one- and two-dimensions, validating the theoretical analysis. Finally, the paper concludes with a summary of findings and suggestions for future work.

**2. Mathematical Modeling: From micro to macro.** In this section, we derive the macroscopic equation (1.6) from microscopic stochastic processes, with a focusing on CTRW framework and overdamped Langevin dynamics. This approach establishes a rigorous connection between macroscopic descriptions and microscopic stochastic dynamics, while also providing a physically meaningful interpretation of the macroscopic model.

**2.1. Model I: Generalized CTRW.** The CTRW model paints a vivid picture for understanding particle diffusion: a particle's journey through space consists of random jumps, each followed by a random waiting time, weaving together a stochastic path full of unexpected pauses and leaps. These microscopic dynamics collectively manifest as rich macroscopic diffusion behaviors, which have been extensively explored in studies such as [9, 31, 42, 52, 53, 59]. We now summarize some key results from these literatures.

Let  $p(t, r)$  denote the probability density function (PDF) of locating the particle at position  $r$  at time  $t$ . Within the CTRW framework, the PDF  $p(t, r)$  admits a compact algebraic representation in the Fourier-Laplace domain, known as the Montroll-Weiss equation [52]

$$(2.1) \quad \widehat{\tilde{p}}_{CTRW}(z, \mathbf{k}) = \frac{1 - \widehat{\psi}(z)}{z} \frac{\tilde{p}_0(\mathbf{k})}{1 - \widehat{\psi}(z)\tilde{\lambda}(\mathbf{k})}, \quad \forall z \in \mathbb{C}, \mathbf{k} \in \mathbb{R}^n,$$

where  $\widehat{\psi}(z)$  is the Laplace transform of the waiting time distribution  $\psi(t)$ ,  $\tilde{\lambda}(\mathbf{k})$  is the Fourier transform of the step size distribution  $\lambda(x)$ , and  $\tilde{p}_0(\mathbf{k})$  is the the Fourier transform of the

initial distribution. This equation forms the cornerstone of the theory of decoupled CTRW. It has been established that when the CTRW is characterized by a power-law waiting time distribution  $\psi(t) \simeq t^{-\alpha-1}$  with  $0 < \alpha < 1$  for  $t > 0$ , and a Gaussian step size distribution with  $\tilde{\lambda}(\mathbf{k}) = \exp(-\mathbf{k}^2) \simeq 1 - |\mathbf{k}|^2$ ,  $\mathbf{k} \in \mathbb{R}^n$  in Fourier space (corresponding to  $\lambda(\mathbf{x}) = (4\pi)^{-1/2} \exp(-\mathbf{x}^2/4)$ ,  $\mathbf{x} \in \mathbb{R}^n$ ), the continuum limit leads to the time-fractional subdiffusion equation. For further details, we refer to [28, 43, 52, 59].

We propose a generalized stable waiting-time distribution in the Laplace domain, given by

$$(2.2) \quad \widehat{\psi}(z) = \exp(-\eta(z)) \simeq 1 - \eta(z), \quad \forall z \in \mathbb{C},$$

where the function  $\eta(z)$  is defined as

$$(2.3) \quad \eta(z) := z^\gamma \left( 1 + az^\alpha + \sum_{k=1}^K a_k z^{\alpha_k} \right) \left( 1 + bz^\beta + \sum_{j=1}^J b_j z^{\beta_j} \right)^{-1},$$

with the relevant parameters specified in (1.5). The expression in (2.2) corresponds to the characteristic function of the waiting-time distribution [3, Pages 16 to 18], which encapsulates complete information about the temporal operators involved. By combining this waiting-time distribution and the Gaussian step size distribution introduced earlier and employing the Montroll-Weiss equation (2.1), we obtain the PDF  $p(t, r)$  in the Fourier-Laplace domain

$$(2.4) \quad \widehat{\tilde{p}}_{CTRW}(z, \mathbf{k}) = \frac{\eta(z)}{z} \frac{1}{1 - (1 - \eta(z))(1 - \mathbf{k}^2)} = \frac{1}{z} \frac{\eta(z) \tilde{p}_0(\mathbf{k})}{\eta(z)(\eta(z)^{-1} - 1)\mathbf{k}^2 + \eta(z)}.$$

Neglecting higher-order terms, we arrive at the asymptotic behavior of the CTRW in the Fourier-Laplace domain, namely  $\widehat{\tilde{p}}_{CTRW}(z, \mathbf{k}) \simeq \widehat{\tilde{p}}(z, \mathbf{k})$ , which satisfies

$$(2.5) \quad \widehat{\tilde{p}}(z, \mathbf{k}) - z^{-1} \tilde{p}_0(\mathbf{k}) = -\mathbf{k}^2 \eta(z)^{-1} \widehat{\tilde{p}}(z, \mathbf{k}).$$

Taking the continuum limit and applying the inverse Fourier-Laplace transform back to the time domain, along with the property  $\mathcal{L}_{z \rightarrow t} \{ {}_0^{RL} \mathcal{D}_t^s \phi(t) \} = z^s \widehat{\phi}(z)$  for all  $s \in (0, 1)$  (see [21]), we readily derive the macroscopic equation (1.4). This result demonstrates that the MT-TFJE (1.4) has a solid physical foundation when the waiting-time distribution in (2.2) is adopted. Moreover, as noted in the introduction, by appropriately choosing the parameters in (1.5), the model can be adapted to describe a wide range of physical models, including the TFJE, classical JE, subdiffusion equation, bifractional diffusion equation, and heat equation. Furthermore, to illustrating the trajectories of particles obeying the waiting-time distribution given by (2.2) and the Gaussian step size distribution, we visualize them based on CTRW, as shown in Fig. 2.1.

A prerequisite for a physically acceptable CTRW model is that the waiting-time distribution  $\psi(t)$  (Eq. (2.2)) is a valid probability density function. The required parameter constraints (Eq. (1.5)) for this are given in the following lemma.

**Proposition 2.1 (Parameter Constraints).** *The waiting time distribution  $\psi(t)$ , defined via its Laplace transform in (2.2), is a PDF if the parameters in (1.5) satisfy conditions  $\beta \leq \gamma$ ,  $\alpha + \gamma + \sum_{k=1}^K \alpha_k \leq 1$ , and  $a_k \cdot b_j \geq 0$ , for all  $k = 0, 1, \dots, K$  and  $j = 0, 1, \dots, J$ , where  $K, J \in \mathbb{N}_+$ .*

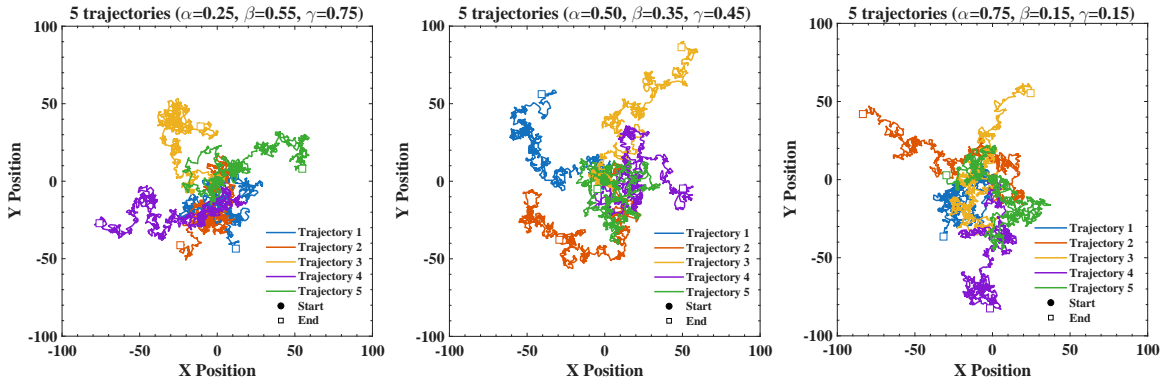


**Figure 2.1.** Two-dimensional trajectories illustrating anomalous diffusion within the CTRW framework. The dynamics follow the generalized waiting time distribution in (2.2) and (2.3), with waiting times distribution numerically generated via Talbot’s numerical inverse Laplace transform algorithm [67]. Parameters are set to  $a = 1$ ,  $b = 100$ , with each trajectory simulated over 1000 steps. The starting point is at the origin.

*Proof.* The proof of this proposition proceeds in two parts. First, we show that the PDF  $\psi(t)$ , defined in the Laplace domain by (2.2), is normalized. This follows directly from the identity  $\int_0^\infty \psi(t)dt = \int_0^\infty e^{-zt}\psi(t)dt|_{z=0} = \widehat{\psi}(z)|_{z=0} = 1$ , which holds for all parameter values given in (1.5).

Second, we demonstrate that  $\psi(t)$  is non-negative under the stated parameter constraints.

A standard method to establish non-negativity of an integrable function  $\varphi(t)$  is to show that  $\hat{\varphi}(\xi)$  is completely monotone (c.m.) for  $\xi = \Re(z) > 0$  (with  $\Re(z)$  denotes the real part of  $z \in \mathbb{C}$ ) [22, pp. 439-442]. Here,  $\hat{\varphi}(\cdot)$  represents the Laplac transform  $\hat{\varphi}(z) = \int_0^\infty e^{-zt}u(t)dt$  of  $\varphi(t)$ . Direct verification in this case is often challenging. Instead, we adopt an indirect approach based on properties of completely monotone functions (CMF), Stieltjes functions (SF), Bernstein functions (BF), and complete Bernstein functions (CBF), as introduced in [5, 7, 8, 59] (see Def. A.1 for definitions). Using this approach, we prove that  $\widehat{\psi}(z) \in \mathcal{CMF}$  for  $\xi = \Re(z) > 0$  under the given parameter constraints. To this end, by Remark A.2 (iv), it suffices to show that  $\eta(\xi) \in \mathcal{CBF}$ .

For  $k = 0, 1, \dots, K$  and  $j = 0, 1, \dots, J$ , from (1.5), the condition  $a_k \cdot b_j \geq 0$  encompasses following cases: (i)  $a_k = 0$  and  $b_j = 0$ ; (ii)  $a_k \geq 0$  and  $b_j = 0$ , or  $a_k = 0$  and  $b_j \geq 0$ ; (iii)  $a_k > 0$  and  $b_j > 0$ . In case (i), the model ML-TFJL simplifies to the JE with constraints  $\alpha + \gamma - \beta < 1$  and  $\beta \leq \gamma$ . The conclusion follows directly from [7, Prop. 1]. For case (ii), consider  $a_k \geq 0$  and  $b_j = 0$ . Then  $\eta(z) := z^\gamma (1 + az^\alpha + \sum_{k=1}^K a_k z^{\alpha_k}) (1 + bz^\beta)^{-1}$ . Define  $[\mathcal{CBF}]^s := \{\hat{\varphi}(\xi)^s : \hat{\varphi}(\xi) \in \mathcal{CBF}, s > 0\}$ , where  $\mathcal{CBF}$  is defined in Remark A.2. Under the constraint  $0 < \alpha + \gamma + \sum_{k=1}^K \alpha_k \leq 1$ , we have  $0 < \alpha + \gamma - \beta < 1$  and  $\beta \leq \gamma$ . From [8, Thm. 1], it follows that  $1 + a\xi^\alpha + \sum_{k=1}^K a_k \xi^{\alpha_k} \in [\mathcal{CBF}]^\alpha$ ,  $\xi^\gamma (1 + b\xi^\beta + \sum_{j=1}^J b_j \xi^{\beta_j})^{-1} \in [\mathcal{CBF}]^\gamma$ , and  $\alpha + \gamma < 1$ . Therefore, by Remark A.2 (iv),  $\eta(\xi) \in \mathcal{CBF}$ . The remaining cases follow similarly, which completes the proof.  $\blacksquare$

The result presented in Prop. 2.1 is fairly general and encompasses several notable cases. For instance, when  $a_k = 0$ ,  $b_j = 0$ , and  $\alpha = \beta = \gamma = 1$ , it follows from [7, Prop. 1] that for  $b/a > 1$ ,  $\eta(\xi) \in \mathcal{CBF}$ , which guarantees that  $\phi(t)$  is a valid PDF. Further discussion of such

special cases can be found in [8, Sec. 4]. In what follows, we restrict attention to parameter sets satisfying the conditions of Prop. 2.1.

**2.1.1. The MSD.** Let  $X(t)$  be the stochastic process described by the generalized CTRW model in Sec. 2.1. A standard method for characterizing particle spreading in diffusion processes is to analyze moments of the propagator, especially the MSD [32]. Below, we investigate the MSD of  $X(t)$  and analyze its asymptotic behavior in both the long- and short-time limits.

First, we recall a useful identity for the moments of stable distributions,  $\langle X^n(t) \rangle = \mathfrak{L}_{z \rightarrow t}^{-1}\{(-i\partial_{\mathbf{k}})^n \hat{p}(z, \mathbf{k})\}|_{\mathbf{k}=0}$ , as given in [3, p.16] or [31, Sec. 3.3]. Then, from (2.4), it follows directly that  $\langle X^0(t) \rangle = \mathfrak{L}_{z \rightarrow t}^{-1}\{1/z\} = 1$ , confirming that the PDF  $p(t, r)$  defined in (2.4) in Fourier-Laplace space is properly normalized.

Next, we analyze the MSD of  $X(t)$ . Following a similar procedure, we obtain  $\langle X^2(t) \rangle = \mathfrak{L}_{z \rightarrow t}^{-1}\{\frac{1}{z} \frac{1-\eta(z)}{\eta(z)}\}$ . Let  $\Theta(z) := \eta(z)/(1-\eta(z))$ . Observing that  $\Theta(z) = \sum_{n=1}^{\infty} \eta(z)^n$  (see [31, Sec.5.1]) and neglecting the higher-order terms, we approximate  $\langle X^2(t) \rangle \simeq \mathfrak{L}_{z \rightarrow t}^{-1}\{1/(z\eta(z))\}$ . Using the definition of  $\eta(z)$  in (2.3), and taking the continuum limit, we derive

$$(2.6) \quad \frac{1}{z\eta(z)} = \frac{1 + bz^{\beta} + \sum_{j=1}^J b_j z^{\beta_j}}{z^{\gamma+1}(1 + az^{\alpha} + \sum_{k=1}^K a_k z^{\alpha_k})} \simeq \begin{cases} \frac{b}{a} z^{\beta-\alpha-\gamma-1}, & z \rightarrow \infty, \\ z^{-\gamma-1}, & z \rightarrow 0. \end{cases}$$

Applying the inverse Laplace transform to (2.6) and using Tauberian's theorem (see [3, Thm.1.5.7]), we obtain the asymptotic behavior of the MSD

$$(2.7) \quad \langle X^2(t) \rangle \simeq \mathfrak{L}_{z \rightarrow t}^{-1}\{1/(z\eta(z))\} \sim \begin{cases} \frac{b}{a} \cdot \frac{t^{\alpha+\gamma-\beta}}{\Gamma(1+\alpha+\gamma-\beta)}, & t \rightarrow 0^+, \\ \frac{t^{\gamma}}{\Gamma(1+\gamma)}, & t \rightarrow +\infty. \end{cases}$$

Based on the preceding analysis, a systematic scaling analysis can be straightforwardly performed. The resulting asymptotic regimes are directly obtained from equation (2.7). In particular, when  $b/a \geq 1$ , the MSD expression in (2.7) encompasses multiple distinct asymptotic scaling laws, highlighting a diverse range of dynamical and scaling crossovers:

- When  $\alpha = \beta = \gamma = 1$ , the model recovers the classical JE, and the MSD satisfies  $\langle X^2(t) \rangle \sim t$  for both  $t \rightarrow 0^+$  and  $t \rightarrow \infty$ . If  $\alpha = \beta = \gamma \neq 1$ , subdiffusion may occur. For instance, when  $\alpha = \beta = \gamma = 1/2$ , the MSD follows  $\langle X^2(t) \rangle \sim t^{1/2}$ , signifying a subdiffusion process.
- When  $\alpha < \beta$ , the system corresponds to the TFJE, indicating an accelerating subdiffusion process. If  $\gamma = 1$ , it signifies a crossover from subdiffusion to normal diffusion.
- When  $\alpha > \beta$ , the process shows retarded subdiffusion if  $\alpha + \gamma - \beta < 1$ , and a transition from superdiffusion to subdiffusion if  $\alpha + \gamma - \beta > 1$ . If  $\alpha > \beta$  and  $\gamma = 1$ , the behavior describes a crossover from superdiffusion to normal diffusion.

The asymptotic behaviors in MSD reported here align with those in [7, 8]. However, our work is distinguished by a simpler derivation that does not heavily rely on the properties of Mittag-Leffler functions.

**2.2. Model II: Overdamped Langevin equation with time-changing.** To capture the intricate dynamics of MT-TFJE given in (1.4), we propose an alternative model via a subordinated coupled, overdamped Langevin system [26]

$$(2.8) \quad \begin{cases} x(t) = y(S(t)), \\ dy(\bar{\tau}) = \sqrt{2D}dW(\bar{\tau}). \end{cases}$$

Here,  $S(t)$  denotes the inverse stable subordinator, defined as  $S(t) = \inf\{\bar{\tau} \geq 0 : T(\bar{\tau}) > t\}$  (see [3, 43] and references therein). The process  $T(\bar{\tau})$  is an nondecreasing stochastic process that serves as a random clock, capturing the distribution of waiting times. Its Laplace exponent is given by  $\mathbb{E}[e^{-zT(\bar{\tau})}] = e^{-\bar{\tau}\eta(z)}$ , where  $\bar{\tau}$  represents operational time. The constant  $D > 0$  is the diffusion coefficient, and  $W(\bar{\tau})$  is an independent Gaussian white noise characterized by the moments  $\langle W(s) \rangle = 0$  and  $\langle W(s_1)W(s_2) \rangle = \delta(s_1 - s_2)$ .

Let  $g(t, r)$  denote the PDF of the stochastic process  $y(\bar{\tau})$ . Then  $g$  satisfies the standard Fokker-Planck equation [26]

$$(2.9) \quad \partial_{\bar{\tau}}g(\bar{\tau}, r) = D\partial_{rr}g(\bar{\tau}, r), \quad \text{with } g(0, r) = p_0(r).$$

Applying the Laplace transform with respect to  $\bar{\tau}$  yields  $s\hat{g}(s, r) - g(0, r) = D\partial_{rr}\hat{g}(s, r)$ , or equivalently,  $\hat{g}(s, r) = (s - D\partial_{rr})^{-1}g(0, r)$ . Now, let  $h(t, \bar{\tau})$  be the PDF of  $S(\tau)$ . Its Laplace transform (with respect to  $t$ ) is given by  $\hat{h}(t, \bar{\tau}) = z^{-1}\eta(z)e^{-\bar{\tau}\eta(z)}$  (see, e.g., [26]). Using the the subordination identity  $p(t, r) = \int_0^\infty h(t, \bar{\tau})g(\bar{\tau}, r)d\bar{\tau}$  (see, e.g., [51]), and taking the Laplace transform with respect to  $t$ , we obtain  $\hat{p}(z, r) = z^{-1}\eta(z)\hat{g}(\eta(z), r)$ . Substituting the expression for  $\hat{g}$  and rearranging yields

$$(2.10) \quad \eta(z)\hat{p}(z, r) - z^{-1}\eta(z)p_0(r) = D\partial_{rr}\hat{p}(z, r).$$

This expression reduces to the Laplace-domain equivalent of (2.5) when  $D = 1$ , consistent with the result obtained from the CTRW model.

Models I and II are constructed to provide a consistent microscopic foundation for the macroscopic MT-TFJE presented in (1.4). By carefully reconciling micro- and macro-scale dynamics, we posit that these models form a versatile and robust framework. This framework not only deepens our theoretical understanding but also paves the way for generalizing and applying such dynamics across various domains in engineering and the physical sciences.

**3. Solution theory.** Having established the microscopic foundations, we now conduct a rigorous mathematical analysis of the macroscopic MT-TFJE. This analysis, focusing on solution regularity and well-posedness, will provide a rigorous foundation for the error estimates of the numerical schemes to follow.

**3.1. Additional notations and function spaces.** For clarity of presentation and without loss of generality, we adopt throughout this paper standard notations and results for Lebesgue spaces  $L^q(\Omega)$  and Sobolev spaces  $W^{m,q}(\Omega)$ , where  $1 \leq q \leq \infty$  and  $m \in \mathbb{N}$ . We define the spatial operator  $\mathcal{A} := -\Delta : H^2(\Omega) \cap H_0^1(\Omega) \rightarrow L^2(\Omega)$  as the negative Laplacian with homogeneous Dirichlet boundary conditions. Let  $(\lambda_j, \varphi_j)_{j \in \mathbb{N}}$  denote its eigenvalues, arranged in non-decreasing order, and the corresponding eigenfunctions normalized in  $L^2(\Omega)$ .

The fractional Sobolev space  $\dot{H}^q(\Omega)$ , for  $q \geq -1$ , is defined as  $\dot{H}^q(\Omega) := \{v \in L^2(\Omega) : \sum_{j=1}^{\infty} \lambda_j^q (v, \varphi_j)^2 < \infty\}$ , equipped with the inner product  $(u, v)_{\dot{H}^q(\Omega)} := \sum_{j=1}^{\infty} \lambda_j^q (u, \varphi_j)(v, \varphi_j)$  and norm  $\|v\|_{\dot{H}^q(\Omega)} := (v, v)_{\dot{H}^q(\Omega)}^{1/2}$ , for all  $u, v \in \text{span}\{\varphi_j\}$  (see, e.g., [1]). One may verify that the spaces  $\dot{H}^q$  form a Hilbert interpolation spaces. In particular,  $\dot{H}^0(\Omega) = L^2(\Omega)$ ,  $\dot{H}^1(\Omega) = H_0^1(\Omega) = \{v \in H^1 : v|_{\partial\Omega} = 0\}$ , a subspace of  $H^1(\Omega)$  where functions vanish on  $\partial\Omega$ , and  $\dot{H}^2(\Omega) = H^2(\Omega) \cap H_0^1(\Omega)$ .

In addition, for  $\theta \in (\pi/2, \pi)$ , we define the sectors

- $\Sigma_{\theta} := \{z \in \mathbb{C} \setminus \{0\}, |\arg(z)| < \theta\}$ ,
- $\Sigma_{\theta, \delta} := \{z \in \mathbb{C} : |z| \geq \delta, \delta > 0, |\arg(z)| < \theta\}$ ,

and the contour

- $\Gamma_{\theta, \delta} := \{z \in \mathbb{C} : |z| = \delta, |\arg(z)| \leq \theta\} \cup \{z \in \mathbb{C} : z = \bar{r}e^{\pm i\theta}, 0 < \delta \leq \bar{r} < \infty\}$ ,

oriented with an increasing imaginary part, where  $i^2 = -1$ .

Based on the above preparations, we now state a useful lemma that will be frequently applied in the construction of the solution theory.

**Lemma 3.1 (Resolvent estimate [4]).** *Let  $\mathcal{A}$  be the negative Laplacian with a homogeneous Dirichlet boundary conditions. For every  $\vartheta \in (0, \pi)$ , there exists a constant  $C > 0$  such that the resolvent operator  $(zI + \mathcal{A})^{-1} : L^2(\Omega) \rightarrow L^2(\Omega)$  satisfies*

$$(3.1) \quad \|(zI + \mathcal{A})^{-1}\|_{L_2(\Omega) \rightarrow L_2(\Omega)} \leq C(1 + |z|)^{-1}, \quad \forall z \in \Sigma_{\vartheta}.$$

Throughout this work, the symbols  $c$  and  $C$  denote generic positive constants that may depend on model parameters but are independent of the functions under consideration. Their values may vary from line to line.

**3.2. Sobolev regularity of the solution.** This section is devoted to establishing the well-posedness and Sobolev regularity of the solution to Problem (1.6).

We begin by applying the Laplace transform to both sides of (1.6) for  $z \in \Sigma_{\theta}$ , where  $\theta \in (\pi/2, \pi)$ , which yields

$$z^{\gamma-1} \left(1 + az^{\alpha} + \sum_{k=1}^K a_k z^{\alpha_k}\right) (z\hat{p}(z) - p_0) + \left(1 + bz^{\beta} + \sum_{j=1}^J b_j z^{\beta_j}\right) \mathcal{A}\hat{p}(z) = \hat{f}(z).$$

Recalling the definition of  $\eta(z)$  from (2.3) and introducing

$$(3.2) \quad \mathcal{H}(z) := z^{-1} \eta(z) (\eta(z)I + \mathcal{A})^{-1},$$

we can express the solution in the Laplace domain as

$$(3.3) \quad \hat{p}(z) = \mathcal{H}(z)p_0 + \left(z^{\gamma-1} + az^{\alpha+\gamma-1} + \sum_{k=1}^K a_k z^{\alpha_k+\gamma-1}\right)^{-1} \mathcal{H}(z) \hat{f}(z).$$

Applying the inverse Laplace transform and invoking Cauchy's theorem along with Remark 3.3, we obtain

$$(3.4) \quad p(t) = \mathcal{E}(t)p_0 + \int_0^t \mathcal{F}(s)f(t-s)ds, \quad t > 0,$$

where the solution operators  $\mathcal{E}(t)$  and  $\mathcal{F}(t) : L^2(\Omega) \rightarrow L^2(\Omega)$ , are defined by

$$(3.5) \quad \mathcal{E}(t) := \frac{1}{2\pi i} \int_{\Gamma_{\theta,\delta}} e^{zt} \mathcal{H}(z) dz, \quad \mathcal{F}(t) := \frac{1}{2\pi i} \int_{\Gamma_{\theta,\delta}} e^{zt} g(z) \mathcal{H}(z) dz,$$

with  $g(z) := (z^{\gamma-1} + az^{\alpha+\gamma-1} + \sum_{k=1}^K a_k z^{\alpha_k+\gamma-1})^{-1}$ . The representation (3.4) is referred to as the *mild solution* of Problem (1.6).

Having derived the solution representation, we now examine the analytic properties of  $\eta(z)$  and  $\mathcal{H}(z)$ , the solution operators  $\mathcal{E}(t)$  and  $\mathcal{F}(t)$ . Understanding these properties is key to establishing a rigorous theory for the problem.

**Lemma 3.2 (Analyticity).** *Let  $\eta(z)$  and  $\mathcal{H}(z)$  be defined as in (2.3) and (3.2), respectively. Assume the parameters in (1.5) satisfy the conditions stated in Prop. 2.1, and that  $\sum_{j=1}^J \beta_j \leq \sum_{k=1}^K \alpha_k$  for  $k = 0, 1, \dots, K$ ,  $j = 0, 1, \dots, J$ , with  $K, J \in \mathbb{N}_+$ . Then, for all  $z \in \Sigma_{\theta,\delta}$  with  $\theta \in (\frac{\pi}{2}, \pi)$  and  $\delta > 1$ , the following hold:*

- (i)  $\eta(z) \in \Sigma_\theta$ , and there exist constants  $c, C > 0$  such that  $c|z|^{\alpha-\beta+\gamma} \leq |\eta(z)| \leq C|z|^{\alpha-\beta+\gamma}$ .
- (ii) The operator  $\mathcal{H}(z) : L^2(\Omega) \rightarrow L^2(\Omega)$  is well-defined and bounded for  $z \in \Sigma_{\theta,\delta}$ , and it belongs to  $\Sigma_\theta$ , satisfying

$$(3.6) \quad \begin{aligned} \|\mathcal{H}(z)\|_{L^2(\Omega) \rightarrow L^2(\Omega)} &\leq C|z|^{-1}, & \|g(z)\mathcal{H}(z)\|_{L^2(\Omega) \rightarrow L^2(\Omega)} &\leq C|z|^{-\alpha-\gamma}, \\ \|\mathcal{A}\mathcal{H}(z)\|_{L^2(\Omega) \rightarrow L^2(\Omega)} &\leq C|z|^{\alpha-\beta+\gamma-1}, & \|g(z)\mathcal{A}\mathcal{H}(z)\|_{L^2(\Omega) \rightarrow L^2(\Omega)} &\leq C|z|^{-\beta}, \end{aligned}$$

where  $g(z) := (z^{\gamma-1} + az^{\alpha+\gamma-1} + \sum_{k=1}^K a_k z^{\alpha_k+\gamma-1})^{-1}$ .

**Proof.** For part (i), define  $\mathcal{N}(z) := 1 + az^\alpha + \sum_{k=1}^K a_k z^{\alpha_k}$  and  $\mathcal{D}(z) := 1 + bz^\beta + \sum_{j=1}^J b_j z^{\beta_j}$ . For  $z \in \Sigma_\theta$ , it is clear that  $\mathcal{D}(z) \neq 0$ . Let  $\overline{\mathcal{D}(z)}$  denote the conjugate of  $\mathcal{D}(z)$ , i.e.,  $\overline{\mathcal{D}(z)} := 1 + b\overline{z}^\beta + \sum_{j=1}^J b_j \overline{z}^{\beta_j}$ . Within the sector  $|\arg(z)| < \theta < \pi$ , the identities  $\overline{z^\beta} = (\overline{z})^\beta$  and  $\overline{z^{\beta_j}} = (\overline{z})^{\beta_j}$  hold. Therefore,  $\overline{\mathcal{D}(z)} = \mathcal{D}(\overline{z}) := 1 + b(\overline{z})^\beta + \sum_{j=1}^J b_j (\overline{z})^{\beta_j}$ . To analyze  $\eta(z)$ , multiply both numerator and denominator by  $\mathcal{D}(\overline{z})$ , yielding

$$\eta(z) = z^\gamma \frac{\mathcal{N}(z)}{\mathcal{D}(z)} = z^\gamma \frac{\mathcal{N}(z)\mathcal{D}(\overline{z})}{\mathcal{D}(z)\mathcal{D}(\overline{z})} = z^\gamma \frac{(1 + az^\alpha + \sum_{k=1}^K a_k z^{\alpha_k})(1 + b(\overline{z})^\beta + \sum_{j=1}^J b_j (\overline{z})^{\beta_j})}{|1 + bz^\beta + \sum_{j=1}^J b_j z^{\beta_j}|^2}.$$

Now, let  $z = |z|e^{i\varphi} \in \Sigma_\theta$  with  $0 \leq \varphi \leq \theta$  (or  $-\theta \leq -\varphi \leq 0$ ), and define  $\mathcal{B} := 1/(\mathcal{D}(z)\mathcal{D}(\overline{z})) = 1/|1 + bz^\beta + \sum_{j=1}^J b_j z^{\beta_j}|^2 > 0$ . Under the parameter conditions from Prop. 2.1 and the assumption  $\sum_{j=1}^J \beta_j \leq \sum_{k=1}^K \alpha_k$ , we have  $\eta(z) = \mathcal{B}|z|^\gamma e^{i\gamma\varphi} (1 + |z|^\alpha e^{i\alpha\varphi} + \sum_{k=1}^K a_k |z|^{\alpha_k} e^{i\alpha_k\varphi}) (1 + \chi^\beta |z|^\beta e^{-i\beta\varphi} + \sum_{j=1}^J b_j |z|^{\beta_j} e^{-i\beta_j\varphi})$ . The argument of  $\eta(z)$  satisfies  $|\arg(\eta(z))| = |\arg(e^{i\gamma\varphi}) + \arg(1 + |z|^\alpha e^{i\alpha\varphi} + \sum_{k=1}^K a_k |z|^{\alpha_k} e^{i\alpha_k\varphi}) + \arg(1 + \chi^\beta |z|^\beta e^{-i\beta\varphi} + \sum_{j=1}^J b_j |z|^{\beta_j} e^{-i\beta_j\varphi})| \leq (\alpha + \gamma + \sum_{k=1}^K \alpha_k)\varphi \leq \theta$ . Hence, for all  $z \in \Sigma_\theta$ , we conclude that  $\eta(z)$  belongs to  $\Sigma_\theta$ .

Next, we analyze the asymptotic behavior of  $\eta(z)$  in the sector  $\Sigma_{\theta,\delta}$ , where  $\theta \in (\frac{\pi}{2}, \pi)$  and  $\delta > 1$ . As  $|z| \rightarrow \infty$ , the dominant terms in  $\mathcal{N}(z)$  and  $\mathcal{D}(z)$  are  $a|z|^\alpha$  and  $b|z|^\beta$ , respectively, implying that  $\eta(z)$  asymptotically behaves like  $|z|^{\alpha+\gamma-\beta}$ . To the existence of constants  $c, C > 0$  such that the desired inequality holds, we divide the region  $\Sigma_{\theta,\delta}$  into two regions: the unbounded part  $\mathbb{O} := \{z \in \Sigma_{\theta,\delta} : |z| > R\}$ , for some sufficiently large  $R > \delta$ , and the compact

part  $\mathbb{K} := \{z \in \Sigma_{\theta, \delta} : \delta \leq |z| \leq R\}$ . We begin with the region  $\mathbb{O}$ . Since  $\alpha_k < \alpha$  and  $\beta_j < \beta$  for all  $k$  and  $j$ , define  $\epsilon := \min_k \{\alpha - \alpha_k\} > 0$ ,  $\iota := \min_j \{\beta - \beta_j\} > 0$ , so that  $\alpha_k \leq \alpha - \epsilon$  and  $\beta_j \leq \beta - \iota$ . Let  $A = \sum_{k=1}^K a_k$  and  $B = \sum_j^J b_j$ . Then for  $|z| > 1$ ,

$$\begin{aligned} |\mathcal{N}(z)| &\leq a|z|^\alpha + 1 + A|z|^{\alpha-\epsilon}, \quad |\mathcal{N}(z)| \geq a|z|^\alpha - 1 - A|z|^{\alpha-\epsilon}, \\ |\mathcal{D}(z)| &\leq b|z|^\beta + 1 + B|z|^{\beta-\iota}, \quad |\mathcal{D}(z)| \geq B|z|^\beta - 1 - B|z|^{\beta-\iota}. \end{aligned}$$

Choose  $R > \delta > 1$  large enough such that  $a|z|^\alpha > 2(1 + A|z|^{\alpha-\epsilon})$  and  $b|z|^\beta > 2(1 + B|z|^{\beta-\iota})$ . Then we obtain  $|\mathcal{N}(z)| \leq (3/2)a|z|^\alpha$ ,  $|\mathcal{N}(z)| \geq (1/2)a|z|^\alpha$ ,  $|\mathcal{D}(z)| \leq (3/2)b|z|^\beta$ , and  $|\mathcal{D}(z)| \geq (1/2)b|z|^\beta$ . It follows that

$$\begin{cases} |\eta(z)| \leq |z|^\gamma \cdot \frac{(3/2)a|z|^\alpha}{(1/2)b|z|^\beta} = \frac{3a}{b}|z|^{\gamma+\alpha-\beta}, \\ |\eta(z)| \geq |z|^\gamma \cdot \frac{(1/2)a|z|^\alpha}{(3/2)b|z|^\beta} = \frac{a}{3b}|z|^{\gamma+\alpha-\beta}. \end{cases}$$

Thus, for  $z \in \mathbb{O}$ , there exist  $c_{\mathbb{O}} = a/3b > 0$  and  $C_{\mathbb{O}} = 3a/b > 0$  such that  $c_{\mathbb{O}}|z|^{\gamma+\alpha-\beta} \leq |\eta(z)| \leq C_{\mathbb{O}}|z|^{\gamma+\alpha-\beta}$ . Now consider the compact set  $\mathbb{K}$ . Since  $\mathcal{D}(z) \neq 0$  and  $\mathcal{N}(z) \neq 0$  on  $\mathbb{K}$ , and  $\eta(z)$  is continuous and nonzero on this closed bounded set, we have  $m_{\mathbb{K}} := \min_{z \in \mathbb{K}} |\eta(z)| > 0$  and  $M_{\mathbb{K}} := \max_{z \in \mathbb{K}} |\eta(z)| < \infty$ . Define  $d(z) := |z|^{\gamma+\alpha-\beta}$ , which is continuous and positive on  $\mathbb{K}$ , so  $c_d := \min_{z \in \mathbb{K}} d(z) > 0$  and  $C_d := \max_{z \in \mathbb{K}} d(z) < \infty$ . The  $|\eta(z)|/d(z)$  is also continuous and positive on  $\mathbb{K}$ , so there exists constants  $c_{\mathbb{K}} = \min_{z \in \mathbb{K}} |\eta(z)|/d(z) > 0$  and  $C_{\mathbb{K}} \max_{z \in \mathbb{K}} |\eta(z)|/d(z) > 0$  such that  $c_{\mathbb{K}}d(z) \leq |\eta(z)| \leq C_{\mathbb{K}}d(z)$ . Finally, taking  $c = \min\{c_{\mathbb{K}}, c_{\mathbb{O}}\} > 0$  and  $C = \max\{C_{\mathbb{K}}, C_{\mathbb{O}}\} > 0$ , we conclude that for all  $z \in \Sigma_{\theta, \delta}$ ,  $c|z|^{\gamma+\alpha-\beta} \leq |\eta(z)| \leq C|z|^{\gamma+\alpha-\beta}$ . This completes the proof of part (i) of Lemma 3.2.

For part (ii), it follows from (i) that  $\eta(z) \in \Sigma_\theta$  for all  $z \in \Sigma_{\theta, \delta}$ . Consequently, by Lemma 3.1, the resolvent operator  $(\eta(z)I + \mathcal{A})^{-1}$  satisfies

$$(3.7) \quad \|(\eta(z)I + \mathcal{A})^{-1}\|_{L^2(\Omega) \rightarrow L^2(\Omega)} \leq C(1 + |\eta(z)|)^{-1}, \quad \forall z \in \Sigma_{\theta, \delta}.$$

Now, consider the identity  $z\eta^{-1}(z)(\eta(z)I + \mathcal{A})u = v$ . Rewriting this, we obtain that  $u = z^{-1}\eta(z)(\eta(z)I + \mathcal{A})^{-1}v$ . Taking the  $L^2$ -norm on both sides and applying the resolvent estimate (3.7) together with the bounds from Lemma 3.2 (i), we deduce  $\|u\|_{L^2(\Omega)} \leq C|z|^{-1}\|v\|_{L^2(\Omega)}$ . This shows that the operator  $H(z) : L^2(\Omega) \rightarrow L^2(\Omega)$  is well-defined for  $z \in \Sigma_{\theta, \delta}$ , and satisfies  $\|\mathcal{H}(z)\|_{L^2(\Omega) \rightarrow L^2(\Omega)} \leq C|z|^{-1}$ . Next, observe that  $\mathcal{A}(\eta(z)I + \mathcal{A})^{-1} = I - \eta(z)(\eta(z)I + \mathcal{A})^{-1}$ . Using this identity and the estimate from Lemma 3.2 (i), we obtain

$$\|\mathcal{A}\mathcal{H}(z)\|_{L^2(\Omega) \rightarrow L^2(\Omega)} = \|\eta(z)z^{-1} - \eta(z)\mathcal{H}(z)\|_{L^2(\Omega) \rightarrow L^2(\Omega)} \leq C|\eta(z)z^{-1}| \leq C|z|^{\alpha-\beta+\gamma-1}.$$

Finally, using the bound  $|g(z)| \leq C|z|^{1-\alpha-\gamma}$ , the remaining estimates in (3.6) follow directly. This completes the proof of part (ii) of Lemma 3.2.  $\blacksquare$

*Remark 3.3.* The solution  $\widehat{p}(r, z)$  in the Laplace domain, defined in (3.3), is analytic for  $z \in \Sigma_\theta$  with  $\theta \in (\pi/2, \pi)$ . Its singularities may arise from two sources, the factor  $z^{-1}$  and the operator  $(\eta(z)I + \mathcal{A})^{-1}$ . According to Lemma 3.2 (i),  $(\eta(z)I + \mathcal{A})^{-1}$  is analytic for  $z \in \Sigma_{\theta, \delta}$ . Thus, the only singularity of  $\widehat{u}(r, z)$  is a simple pole at  $z = 0$  introduced by the factor  $z^{-1}$ .

From now on, unless otherwise specified, we take  $\theta \in (\frac{\pi}{2}, \pi)$ . Next, we employ the Laplace transform method to establish the Sobolev regularity of the solution to Problem (1.6).

**Lemma 3.4 (Prior estimates).** *Let  $\mathcal{E}(t)$  and  $\mathcal{F}(t)$  be defined as in (3.5). Assume the parameters in (1.5) satisfy the conditions stated in Lemma 3.2. Then for  $t > 0$ ,  $m \in \mathbb{N}_+$ , and  $z \in \Sigma_{\theta, \delta}$  with  $\theta \in (\frac{\pi}{2}, \pi)$  and  $\delta > 1$ , the following statements are valid:*

(i) *The operator  $\mathcal{E}(t)$  satisfies*

$$(3.8) \quad \|\mathcal{E}(t)\|_{\Psi} + t^m \|\partial_t^m \mathcal{E}(t)\|_{\Psi} + t^{m+\alpha-\beta+\gamma} \|\mathcal{A} \partial_t^m \mathcal{E}(t)\|_{\Psi} \leq C,$$

where  $\|\cdot\|_{\Psi}$  denotes the  $L^2(\Omega) \rightarrow L^2(\Omega)$  operator norm.

(ii) *The operator  $\mathcal{F}(t)$  satisfies*

$$(3.9) \quad t^{1-\alpha-\gamma} \|\mathcal{F}(t)\|_{\Psi} + t^{m+1-\alpha-\gamma} \|\partial_t^m \mathcal{F}(t)\|_{\Psi} + t^{m+1-\beta} \|\mathcal{A} \partial_t^m \mathcal{F}(t)\|_{\Psi} \leq C.$$

*Proof.* For part (i), using Lemma 3.2 and the definition of  $\mathcal{E}(t)$ , we take  $\delta = 1/t$  for  $z \in \Sigma_{\theta, \delta}$ . The following estimates hold

$$\begin{aligned} \|\mathcal{E}(t)\|_{L^2(\Omega) \rightarrow L^2(\Omega)} &\leq c \int_{\Gamma_{\theta, \delta}} e^{t|z| \cos(\theta)} \|\mathcal{H}(z)\|_{L^2(\Omega) \rightarrow L^2(\Omega)} |dz| \leq c \int_{\Gamma_{\theta, \delta}} e^{t|z| \cos(\theta)} |z|^{-1} |dz| \\ &\leq C \int_{\delta}^{\infty} e^{tr \cos(\theta)} r^{-1} dr + C \int_{-\theta}^{\theta} e^{\delta t \cos(\varphi)} d\varphi \\ &\quad (\text{let } s = tr, \text{ with } s \in (1, \infty) \text{ and } r = s/t) \\ &\leq C \int_1^{\infty} e^{s \cos \theta} s^{-1} ds + C \int_{-\theta}^{\theta} e^{\delta T} d\varphi \leq C. \end{aligned}$$

Similarly, for the time derivative, we have

$$\|\partial_t \mathcal{E}(t)\|_{L^2(\Omega) \rightarrow L^2(\Omega)} \leq C \int_{\Gamma_{\theta, \delta}} e^{t|z| \cos(\theta)} |z| \|\mathcal{H}(z)\|_{L^2(\Omega) \rightarrow L^2(\Omega)} |dz| \leq C t^{-1}.$$

By similar reasoning, we obtain  $\|\partial_t^m \mathcal{E}(t)\|_{L^2(\Omega) \rightarrow L^2(\Omega)} \leq C t^{-m}$ .

For the operator  $\mathcal{A} \partial_t^m \mathcal{E}(t)$ , we have

$$\|\mathcal{A} \partial_t^m \mathcal{E}(t)\|_{L^2(\Omega) \rightarrow L^2(\Omega)} \leq C \int_{\Gamma_{\theta, \delta}} e^{t|z| \cos(\theta)} |z|^m \|\mathcal{A} \mathcal{H}(z)\|_{L^2(\Omega) \rightarrow L^2(\Omega)} |dz| \leq C t^{\beta-\alpha-\gamma-m}.$$

This completes the proof of part (i) of Lemma 3.4. Part (ii) follows by similar arguments. ■

We now turn to analyze the Sobolev regularity of the solution to Problem (1.6). The main result is stated in the following theorem.

**Theorem 3.5 (Sobolev regularity).** *Let  $m \in \mathbb{N}_+$ , and let  $p(t)$  be the solution to Problem (1.6). Assume the parameters in (1.5) satisfy the conditions of Lemma 3.2. Then for  $0 < t \leq T$  and  $l = 0, 1$ , the following estimates hold:*

(i) If  $p_0 \in L^2(\Omega)$ ,  $f(t, r) \in AC([0, T]; L^1(\Omega))$  and  $\partial_t^j p(t, r)|_{t=0} := p^{(j)}(0) \in C(0, T; L^2(\Omega))$  for  $j = 0, 1, \dots, m-1$ , with  $\int_0^t \|\partial_s^m f(s, r)\|_{L^2(\Omega)} ds < \infty$ , then there exists  $C > 0$  such that

$$\begin{aligned} \|\mathcal{A}^l \partial_t^m p(t)\|_{L^2(\Omega)} &\leq C \left( \sum_{j=0}^{m-1} t^{(1-l)(\alpha+\gamma)+l\beta+j-m} \|f^{(j)}(0)\|_{L^2(\Omega)} \right. \\ &\quad \left. + t^{(1-l)(\alpha+\gamma)+l\beta-1} * \|\partial_t^m f(t)\|_{L^2(\Omega)} + t^{l(\beta-\alpha-\gamma)-m} \|p_0\|_{L^2(\Omega)} \right). \end{aligned}$$

(ii) If, in addition,  $p_0 \in D(\mathcal{A}) = \dot{H}^2(\Omega)$ , then

$$\begin{aligned} \|\mathcal{A}^l \partial_t^m p(t)\|_{L^2(\Omega)} &\leq C \left( \sum_{j=1}^{m-1} t^{(1-l)(\alpha+\gamma)+l\beta+j-m} \|f^{(j)}(0)\|_{L^2(\Omega)} \right. \\ &\quad \left. + t^{(1-l)(\alpha+\gamma)+l\beta-1} * \|\partial_t^m f(t)\|_{L^2(\Omega)} + t^{(1-l)(\alpha-\beta+\gamma)-m} \|p_0\|_{\dot{H}^2(\Omega)} \right). \end{aligned}$$

In part (i),  $AC([0, T])$  denotes the space of absolutely continuous functions on  $[0, T]$ , and the symbol ‘\*’ denotes temporal convolution.

*Proof.* For part (i), let  $m \in \mathbb{N}_+$  and  $p_0 \in L^2(\Omega)$ . Starting from the integral representation of the solution in the Laplace domain, we have  $p^{(m)}(t) = \frac{1}{2\pi i} \int_{\Gamma_{\theta, \delta}} e^{zt} z^m (\mathcal{H}(z)p_0 + g(z)\mathcal{H}(z)\widehat{f}(z)) dz$ , where  $g(z) := (z^{\gamma-1} + az^{\alpha+\gamma-1} + \sum_{k=1}^K a_k z^{\alpha_k+\gamma-1})^{-1}$ . This yields

$$\|\partial_t^m p(t)\|_{L^2(\Omega)} \leq C \|\partial_t^m \mathcal{E}(t)\|_{L^2(\Omega)} \|p_0\|_{L^2(\Omega)} + C \|\mathcal{F}(t) * f(t)\| := \widetilde{I} + \widetilde{II}.$$

From Lemma 3.4, it follows that  $\widetilde{I} \leq Ct^{-m} \|p_0\|_{L^2(\Omega)}$ . Under the given conditions on  $f(t)$ , we apply Taylor expansion to write  $\widehat{f}(z) = \sum_{j=0}^{m-1} f^{(j)}(0)z^{-j-1} + \widehat{f}^{(m)}(z)z^{-m}$  with  $z \in \Sigma_\theta$ . Then,

$$\begin{aligned} \widetilde{II} &\leq C \int_{\Gamma_{\theta, \delta}} e^{|z|t \cos(\theta)} |z|^m \|g(z)\mathcal{H}(z)\|_{L^2(\Omega) \rightarrow L^2(\Omega)} \|\widehat{f}(z)\|_{L^2(\Omega)} |dz| \\ &\leq C \int_{\Gamma_{\theta, \delta}} e^{|z|t \cos(\theta)} |z|^{m-\alpha-\gamma} \left( \sum_{j=0}^{m-1} \|f^{(j)}(0)\|_{L^2(\Omega)} |z|^{-j-1} + \|\widehat{f}^{(m)}(z)\|_{L^2(\Omega)} |z|^{-m} \right) |dz| \\ &\leq C \sum_{j=0}^{m-1} t^{\alpha+\gamma+j-m} \|f^{(j)}(0)\|_{L^2(\Omega)} + Ct^{\alpha+\gamma-1} * \|\partial_t^m f(t)\|_{L^2(\Omega)}. \end{aligned}$$

Combining the estimates for  $\widetilde{I}$  and  $\widetilde{II}$  yields the desired bound for  $\partial_t^m p(t)$ . For the estimate of  $\mathcal{A}\partial_t^m p(t)$ , we apply a similar approach to derive

$$\begin{aligned} \|\mathcal{A}\partial_t^m p(t)\|_{L^2(\Omega)} &\leq C \left( \|\mathcal{A}\partial_t^m \mathcal{E}(t)\|_{L^2(\Omega) \rightarrow L^2(\Omega)} \|p_0\|_{L^2(\Omega)} + \frac{1}{2\pi} \int_{\Gamma_{\theta, \delta}} e^{|z|t \cos(\theta)} |z|^m \|g(z)\mathcal{A}\mathcal{H}(z)\widehat{f}(z)\|_{L^2(\Omega)} |dz| \right) \\ &\leq Ct^{\beta-\alpha-\gamma-m} \|p_0\|_{L^2(\Omega)} + C \left( \sum_{j=0}^{m-1} t^{\beta+j-m} \|f^{(j)}(0)\|_{L^2(\Omega)} + t^{\beta-1} * \|\partial_t^m f(t)\|_{L^2(\Omega)} \right). \end{aligned}$$

These estimates complete the proof of Thm. 3.5 (i).

For part (ii), since  $\mathcal{A}$  is closed and self-adjoint, it commutes with the resolvent  $(\eta(z)I + \mathcal{A})^{-1}$ , and hence with  $\mathcal{H}(z)$ . From (3.4), we have

$$\begin{aligned}\partial_t^m p(t) &= \frac{1}{2\pi i} \int_{\Gamma_{\theta,\delta}} e^{zt} z^m \mathcal{A}^{-1} \mathcal{H}(z) \mathcal{A} p_0 dz + \frac{1}{2\pi i} \int_{\Gamma_{\theta,\delta}} e^{zt} z^m g(z) \mathcal{H}(z) \widehat{f}(z) dz \\ &= \frac{1}{2\pi i} \int_{\Gamma_{\theta,\delta}} e^{zt} z^{m-1} \eta(z) \mathcal{A}^{-1} (\eta(z)I + \mathcal{A})^{-1} \mathcal{A} p_0 dz + \frac{1}{2\pi i} \int_{\Gamma_{\theta,\delta}} e^{zt} z^m g(z) \mathcal{H}(z) \widehat{f}(z) dz.\end{aligned}$$

Now, using the identity  $\eta(z) \mathcal{A}^{-1} (\eta(z)I + \mathcal{A})^{-1} = \mathcal{A}^{-1} - (\eta(z)I + \mathcal{A})^{-1}$ , and the fact that  $\int_{\Gamma_{\theta,\delta}} z^{m-1} e^{zt} dz = 0$  for  $m \geq 1$  (since it represents the inverse Laplace transform of  $z^{m-1}$ , which is a distribution supported at  $t = 0$ ), it follows from Lemmas 3.2 and 3.4 that

$$\begin{aligned}\|\partial_t^m p(t)\|_{L^2(\Omega)} &\leq C \left\| \int_{\Gamma_{\theta,\delta}} e^{zt} z^{m-1} (I - (\eta(z)I + \mathcal{A})^{-1} \mathcal{A}) p_0 dz \right\|_{L^2(\Omega)} + C \left\| \int_{\Gamma_{\theta,\delta}} e^{zt} z^m g(z) \mathcal{H}(z) \widehat{f}(z) dz \right\|_{L^2(\Omega)} \\ &\leq C t^{\alpha+\gamma-\beta-m} \|p_0\|_{\dot{H}^2(\Omega)} + C \left( \sum_{j=0}^{m-1} t^{\alpha+\gamma+j-m} \|f^{(j)}(0)\|_{L^2(\Omega)} + t^{\alpha+\gamma-1} * \|\partial_t^m f(t)\|_{L^2(\Omega)} \right).\end{aligned}$$

The estimate for  $\mathcal{A} \partial_t^m p(t)$  follows similarly,

$$\begin{aligned}\|\mathcal{A} \partial_t^m p(t)\|_{L^2(\Omega)} &\leq \left\| \frac{1}{2\pi i} \int_{\Gamma_{\theta,\delta}} e^{zt} z^{m-1} \mathcal{A} (\eta(z)I + \mathcal{A})^{-1} \mathcal{A} p_0 dz \right\|_{L^2(\Omega)} + C \left\| \int_{\Gamma_{\theta,\delta}} e^{zt} z^m g(z) \mathcal{A} \mathcal{H}(z) \widehat{f}(z) dz \right\|_{L^2(\Omega)} \\ &\leq C t^{-m} \|p_0\|_{\dot{H}^2(\Omega)} + C \left( \sum_{j=0}^{m-1} t^{\beta+j-m} \|f^{(j)}(0)\|_{L^2(\Omega)} + t^{\beta-1} * \|\partial_t^m f(t)\|_{L^2(\Omega)} \right).\end{aligned}$$

These estimations complete the proof of the Thm. 3.5 (ii). ■

For  $m = 0$ , subject to stronger regularity conditions on  $f$ , the problem admits a solution with improved regularity.

**Theorem 3.6 (Sobolev regularity).** *Let  $p_0 \equiv 0$  and let  $p(t)$  be the solution to Problem (1.6). Assume the parameters in (1.5) satisfy the conditions stated in Lemma 3.2. Then the following estimates hold with constants  $C > 0$  that may vary between inequalities:*

(i) *If  $f \in L^1(0, T; L^2(\Omega))$ , then for all  $t \in (0, T]$  and  $l = 0, 1$ ,*

$$(3.10) \quad \|\mathcal{A}^l p(t)\|_{L^2(\Omega)} \leq C \int_0^t (t-s)^{\alpha+\gamma-1-l(\alpha+\gamma-\beta)} \|f(s)\|_{L^2(\Omega)} ds.$$

(ii) *If  $f \in L^1(0, T; \dot{H}^2(\Omega))$ , then for all  $t \in (0, T]$  and  $l = 0, 1$ ,*

$$(3.11) \quad \|\mathcal{A}^l p(t)\|_{L^2(\Omega)} \leq C \int_0^t (t-s)^{\alpha+\gamma-1} \|f(s)\|_{L^2(\Omega)} ds.$$

*Proof.* A direct application of the estimates in Lemma 3.2, following the technique of Lemma 3.4, yields the results.  $\blacksquare$

According to Theorems 3.5 and 3.6, the solution  $p(t, r)$  of Problem (1.6) exhibits a singularity at the origin. When  $p_0 = 0$ , enhancing the temporal regularity of the source term improves the solution's regularity. Moreover, since  $\mathcal{A}$  is a positive and self-adjoint, we have the norm equivalence  $\|\mathcal{A}^\nu u\|_{L^2(\Omega)} \approx \|u\|_{\dot{H}^{2\nu}(\Omega)}$  for  $\nu > 0$ . Using this equivalence and applying Sobolev interpolation to the estimates in Theorems 3.5 and 3.6, we obtain the following result.

**Corollary 3.7.** *Let  $p(t)$  be the solution to Problem (1.6). Assume the parameters in (1.5) satisfy the conditions of Lemma 3.2. Then the following estimates hold:*

(i) *Let  $f \equiv 0$  and  $p_0 \in \dot{H}^q(\Omega)$ . Then there exists a constant  $C > 0$  such that*

$$(3.12) \quad \|\partial_t^m p(t, r)\|_{\dot{H}^p(\Omega)} \leq C t^{-m-(\alpha+\gamma-\beta)(p-q)/2} \|p_0\|_{\dot{H}^q(\Omega)}, \quad \text{for } t > 0.$$

*where either  $m = 0$  and  $0 \leq q \leq p \leq 2$ , or  $m > 0$  and  $0 \leq q, p \leq 2$ .*

(ii) *Let  $p_0 \equiv 0$  and  $f \in L^1(0, T; \dot{H}^q(\Omega))$ . Then there exists a constant  $C > 0$ , such that*

$$(3.13) \quad \|p(t, r)\|_{\dot{H}^p(\Omega)} \leq C \int_0^t (t-s)^{\alpha+\gamma-1-(\alpha+\gamma-\beta)(p-q)/2} \|f(s)\|_{\dot{H}^q(\Omega)} ds, \quad \text{for } t > 0.$$

**Remark 3.8 (Well-posedness).** To establish the well-posedness of Problem (1.6), it is necessary to impose stronger assumptions on the source term  $f$ , in particular Lipschitz continuity in time. Based on the mild solution representation (3.4), one can construct a solution mapping and verify its bijectivity, continuity, and contraction properties in  $L^p(\Omega)$  for  $p \geq 1$ . The existence and uniqueness of a local mild solution then follow from an application of the Banach fixed-point theorem. Extending this to global well-posedness requires the incorporation of an energy functional; the subsequent analysis is straightforward in light of the prior estimates and will not be elaborated further.

**4. Spatio-temporal spectral accuracy CIM-CLG.** Having established the well-posedness and regularity results for the MT-TFJE, we now turn to its numerical approximation and dynamical properties. We introduce a novel scheme achieving spatio-temporal spectral accuracy, the CIM-CLG algorithm, and present a detailed analysis of its convergence and stability. The discussion commences with the temporal semi-discretization.

**4.1. Semidiscrete CIM.** We present the temporal semi-discrete approximation for MT-TFJE via the contour integral method (CIM), accompanied by a comprehensive error study that encompasses the scheme's convergence and the selection of optimal contour parameters.

**4.1.1. Developing the semidiscrete CIM.** The contour integral method (CIM), originally introduced for the numerical approximation of the inverse Laplace transform [67], has found extensive applications in various fields [14, 15, 34, 39, 44, 49, 50], demonstrating its versatility and effectiveness. The method is based on deforming the Bromwich contour. While the standard contour is a vertical line that leads to challenges such as high-frequency oscillations in the integrand, deforming it into a contour within the left half-plane (as illustrated in Fig. 4.1 (c) and supported by [35, 38, 43, 69]) results in exponential decay due to the factor  $e^{zt}$ , thereby enhancing the convergence rate of the numerical quadrature.

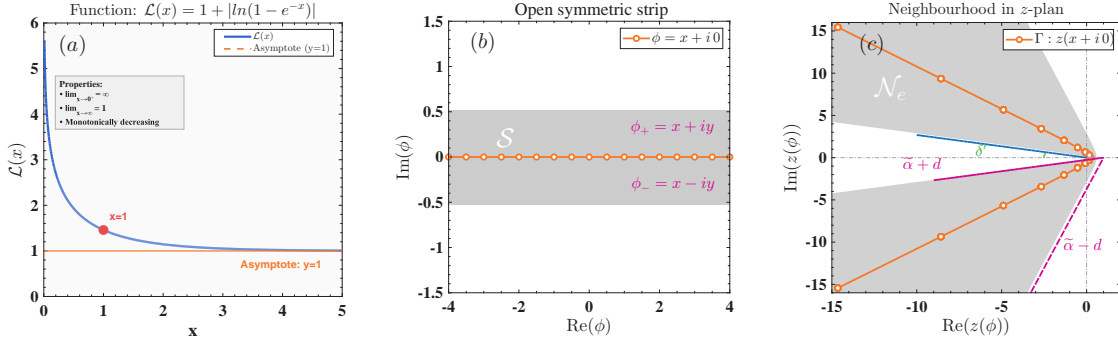


**Figure 4.1.** Illustration of auxiliary function  $L(x)$ , the open symmetric strip  $\mathcal{S}$ , and its neighbourhood  $\mathcal{N}_e$  in the  $z$ -plan. (a) Monotonic decrease of  $L(x)$ . (b) and (c) display the images of  $\mathcal{S}$  under the conformal mapping  $z(\phi)$  defined by (4.1). The upper half of  $\mathcal{S}$  (with  $y > 0$ ) maps to the shaded interior region enclosed by  $z(x + i0)$  within  $\mathcal{N}_e$ ; as  $y$  increases,  $z(\phi)$  approaches the negative real axis. Conversely, the lower half of  $\mathcal{S}$  (with  $y < 0$ ) maps to the exterior shaded region outside  $z(x + i0)$  in  $\mathcal{N}_e$ ; as  $y$  decreases,  $z(\phi)$  converges toward a vertical line;  $|y| \leq d$ , where  $d := \min\{\tilde{\alpha}, \frac{\pi}{2} - \tilde{\alpha} - \delta'\}$  and  $0 < \tilde{\alpha} - d < \tilde{\alpha} + d < \frac{\pi}{2} - \delta'$ . Parameters for (b) and (c):  $\alpha = \pi/4$ ,  $\mu = 0.8$ , and  $\delta = \pi/12$ .

In line with the idea of CIM, we choose the left branch of a hyperbola as the integral contour (see, e.g., [38, 39, 43, 44, 69]). This contour can be parameterized as

$$(4.1) \quad \Gamma : z(\phi) = \mu(1 + \sin(i\phi - \tilde{\alpha})), \quad \forall \phi \in \mathcal{S},$$

where  $\mu > 0$  and  $\tilde{\alpha} > 0$  are parameters to be determined, and  $\mathcal{S}$  denotes an open symmetric strip (see Fig. 4.1 (b)), defined by  $\mathcal{S} := \{\phi = x + iy, |y| \leq d\}$ , with  $d := \min\{\tilde{\alpha}, \frac{\pi}{2} - \tilde{\alpha} - \delta'\}$ , satisfying  $0 < \tilde{\alpha} - d < \tilde{\alpha} + d < \frac{\pi}{2} - \delta'$  (see Fig. 4.1 (c)). Here,  $\delta'$  represents the inclination angle of the asymptote of the hyperbola (4.1). For further discussion of this strip, we refer to our previous works [43, 44]. The conformal mapping  $z(\phi)$  transforms the open strip  $\mathcal{S}$  into a neighbourhood in the complex  $z$ -plan, denoted by  $\mathcal{N}_e := \{z(\phi) \in \mathbb{C} : \phi \in \mathcal{S}\}$  (see Fig. 4.1 (c)). According to Remark 3.3, for a fixed  $\delta' > 0$ , we have  $\mathcal{N}_e \subseteq \Sigma_\theta$ , and the integrand  $\hat{p}(z, r)$  is analytic for  $z(\phi) \in \mathcal{N}_e$ . Therefore, the integral (3.4) can be written as

$$(4.2) \quad p(t, r) = I := \int_{-\infty}^{+\infty} u(t, r, \phi) d\phi, \quad \text{where } u(t, r, \phi) := \frac{1}{2\pi i} e^{z(\phi)t} \hat{p}(r, z(\phi)) z'(\phi),$$

and  $\hat{p}(r, z)$  is defined in (3.3).

Given that  $f \in L^1(0, T; L^2(\Omega))$ , the Schwarz reflection principle implies that  $\hat{f}(\bar{z}) = \overline{\hat{f}(z)}$ . Since the integral contour  $\Gamma$  is symmetric with respect to real axis and  $\hat{p}(r, z(\phi)) = \overline{\hat{p}(r, z(\phi))}$ , applying the midpoint rule to approximate the integral (4.2) with a uniform step-spacing  $\tau > 0$  in  $\phi$  yields the following temporal semi-discrete scheme for Problem (1.6), that is

$$(4.3) \quad p^N(t, r) = I_{\tau; N} := \tau \sum_{k=1-N}^{N-1} u(t, \phi_k) = \frac{\tau}{\pi} \text{Im} \left\{ \sum_{k=0}^{N-1} e^{z_k t} \hat{p}(z_k, r) z'_k \right\},$$

where  $z_k = z(\phi_k)$ ,  $z'_k = z'(\phi_k)$  and  $\phi_k = (k + 1/2)\tau$  for  $k = 0, 1, \dots, N - 1$ . This scheme is straightforward to implement and allows the solution at each time point to be computed independently of previous time steps, facilitating efficient parallel computation.

**4.1.2. Error estimates under lower regularity.** Here, we analyze the error of the CIM (4.3) under the assumption that  $f(t) \in L^1(0, T)$ . This condition ensures the analytic extension of the Laplace transform  $\widehat{f}(z)$  into the sector  $\Sigma_\theta$ , enabling error estimates to be formulated directly in terms of  $\widehat{f}(z)$  rather than  $f(t)$  (see [43, 49]). For a region  $\mathbb{D} \subseteq \Sigma_\theta$ , we define the norm  $\|\widehat{f}(z)\|_{(\mathbb{D}; L^2(\Omega))} = \sup_{z \in \mathbb{D}} \|\widehat{f}(z)\|_{L^2(\Omega)}$ .

Taking  $\mathbb{D} = \mathcal{N}_e$ , we recall the following result from [38]:

**Lemma 4.1 (Auxiliary function).** *For  $x > 0$ , define  $\mathcal{L}(x) = 1 + |\ln(1 - e^{-x})|$ . Then for any  $s > 0$  and  $\sigma > 0$ , the following inequalities hold*

$$(4.4) \quad \int_0^{+\infty} e^{-s \cosh(x)} dx \leq \mathcal{L}(s), \quad \int_\sigma^{+\infty} e^{-s \cosh(x)} dx \leq (1 + \mathcal{L}(s)) e^{-s \cosh(\sigma)}.$$

Note that  $\mathcal{L}(x)$  is a decreasing function, with  $\mathcal{L}(x) \rightarrow 1$  as  $x \rightarrow \infty$ , and  $\mathcal{L}(x) \sim |\ln(x)|$  as  $x \rightarrow 0^+$ ; see Fig. 4.1 (a) for an illustration. Based on this result, the integrand  $u(t, r, \phi)$  defined in (4.2) satisfies the following property.

**Lemma 4.2 (Super-exponential decay).** *Let  $u(t, r, \phi)$  be defined as in (4.2), with  $z(\phi) \in \mathcal{N}_e \subseteq \Sigma_\theta$ . Suppose  $t_0 \leq t \leq t_1$ , where  $t_0 > 0$  and  $\Lambda := t_1/t_0 \geq 1$ . If  $p_0 \in L^2(\Omega)$  and  $\|\widehat{f}(z)\|_{(\mathcal{N}_e, L^2(\Omega))} < \infty$ , then there exists a constant  $C > 0$  such that for all  $\phi = x \pm iy \in \mathcal{S}$ ,*

$$(4.5) \quad \|u(t, r, \phi)\|_{L^2(\Omega)} \leq CQ \frac{e^{\mu t_0 \Lambda}}{t_0^{1-\alpha-\gamma}} \left( \|p_0\|_{L^2(\Omega)} + \|\widehat{f}(z)\|_{(\mathcal{N}_e; L^2(\Omega))} \right) e^{-(1-\nu)\mu t_0 \sin(\tilde{\alpha}-d) \cosh x},$$

where,  $Q := \frac{1}{2\pi} \left( \frac{1-\alpha-\gamma}{\nu \sin(\tilde{\alpha}-d) e^{\nu \mu t_0 \sin(\tilde{\alpha}-d)/(1-\alpha-\gamma)}} \right)^{1-\alpha-\gamma} \sqrt{\frac{1+\sin(\tilde{\alpha}+d)}{1-\sin(\tilde{\alpha}+d)}}$  and  $\nu \in (0, 1)$ .

*Proof.* For a detailed proof, see Appendix B. ■

Next, we introduce two auxiliary series to characterize errors arising in the CIM (4.3):

- $I_\tau := \tau \sum_{k=-\infty}^{\infty} u(t, r, \phi_k)$ ,
- $I_{\tau;N;\varepsilon} = \tau \sum_{k=1-N}^{N-1} u(t, r, \phi_k)(1 + \varepsilon_k)$ .

These allow us to decompose the error of the CIM scheme (4.3) as follows:

$$(4.6) \quad \begin{aligned} E_N &:= \|p(t, r) - p^N(t, r)\|_{L^2(\Omega)} \\ &\leq \|I - I_\tau\|_{L^2(\Omega)} + \|I_\tau - I_{\tau;N}\|_{L^2(\Omega)} + \|I_{\tau;N} - I_{\tau;N;\varepsilon}\|_{L^2(\Omega)} =: \mathcal{D}_e + \mathcal{T}_e + \mathcal{R}_e, \end{aligned}$$

where  $\mathcal{D}_e := \|I - I_\tau\|_{L^2(\Omega)}$  denotes the discretization error,  $\mathcal{T}_e := \|I_\tau - I_{\tau;N}\|_{L^2(\Omega)}$  represents the truncation error,  $\mathcal{R}_e := \|I_{\tau;N} - I_{\tau;N;\varepsilon}\|_{L^2(\Omega)}$  is the round-off error with  $|\varepsilon_k| < \varepsilon$  being relative errors for all  $k = \pm 1, \pm 2, \dots, \pm(N-1)$ . Here,  $\varepsilon$  is a specified accuracy used in auxiliary computations, such as solving linear systems. For further discussions, we refer to [39, 43].

Based on the decay property established in Lemma 4.2 and the technical proofs in [38, 39, 43], it can be demonstrated that for  $t_0 \leq t \leq \Lambda t_0$  with  $t_0 > 0$  and  $\Lambda = t_1/t_0$ , the errors  $\mathcal{D}_e$  and  $\mathcal{T}_e$  satisfy the following uniform estimate:

$$(4.7) \quad \begin{aligned} \mathcal{D}_e + \mathcal{T}_e &\leq \frac{CQ}{t_0^{1-\alpha-\gamma}} \mathcal{L}((1-\nu)\mu t_0 \sin(\tilde{\alpha}-d)) \left( \|p_0\|_{L^2(\Omega)} + \|\widehat{f}(z)\|_{(\mathcal{N}_e; L^2(\Omega))} \right) \\ &\times e^{\mu \Lambda t_0} \left( \frac{1}{e^{2\pi \tilde{d}/\tau} - 1} + \frac{1}{e^{(1-\nu)\mu t_0 \sin(\tilde{\alpha}-\tilde{d}) \cosh(N\tau)}} \right), \quad \forall \nu \in (0, 1). \end{aligned}$$

Additionally, the round-off error  $\mathcal{R}_e$  is uniformly bounded by

$$(4.8) \quad \begin{aligned} \mathcal{R}_e &\leq \tau \sum_{k=1-N}^{N-1} \|u(t, \phi_k)\|_{L^2(\Omega)} |\varepsilon_k| \leq 2\epsilon\tau \sum_{k=0}^{N-1} \|u(t, \phi_k)\|_{L^2(\Omega)} \\ &\leq \frac{CQ}{t_0^{1-\alpha-\gamma}} \mathcal{L}((1-\nu)\mu t_0 \sin(\tilde{\alpha} - d)) \left( \|p_0\|_{L^2(\Omega)} + \|\hat{f}(z)\|_{(\mathcal{N}_e; L^2(\Omega))} \right) e^{\mu\Lambda t_0} \varepsilon. \end{aligned}$$

Let  $\varrho \in (0, 1)$  be a free parameter. Choosing

$$(4.9) \quad \tau = \frac{a(\varrho)}{N}, \quad \mu = \frac{2\pi\tilde{d}N(1-\varrho)}{t_0\Lambda a(\varrho)}, \quad \text{with } a(\varrho) := \cosh^{-1} \left( \frac{\Lambda}{(1-\varrho)\sin(\tilde{\alpha} - d)} \right),$$

we can rewrite the estimate (4.7) as

$$(4.10) \quad \mathcal{D}_e + \mathcal{T}_e \leq CQ \frac{\mathcal{L}((1-\nu)\mu t_0 \sin(\tilde{\alpha} - d))}{t_0^{1-\alpha-\gamma}} \left( \|p_0\|_{L^2(\Omega)} + \|\hat{f}(z)\|_{(\mathcal{N}_e; L^2(\Omega))} \right) e^{\mu\Lambda t_0} \frac{2\varepsilon_N(\varrho)}{1-\varepsilon_N(\varrho)},$$

where  $\varepsilon_N(\varrho) := \exp\left(-\frac{2\pi dN}{a(\varrho)}\right)$ . Combining (4.8) and (4.10), we obtain the overall error bound for  $E_N$  in the CIM scheme (4.3), as stated in the following theorem.

**Theorem 4.3 (Convergence).** *Let  $p(t)$  be the solution to Problem (1.6), and let  $p^N(t)$  be its numerical approximation given by (4.3) with the parameters satisfying the condition states in Lem 3.2. Assume  $\Lambda > 1$ ,  $0 < \tilde{\alpha}, \delta' < \pi/2$ , and for any  $t_0 > 0$  with  $t_0 \leq t \leq \Lambda t_0$ ,  $0 < \varrho < 1$ , if  $p_0 \in L^2(\Omega)$ ,  $\|\hat{f}(z)\|_{(\mathcal{N}_e; L^2(\Omega))} < \infty$ , and parameters  $\tau, \mu$  are chosen according to (4.9), then the error  $E_N = \|p(t) - p^N(t)\|_{L^2(\Omega)}$  satisfies*

$$E_N \leq CQ \frac{\mathcal{L}((1-\nu)\mu t_0 \sin(\tilde{\alpha} - d))}{t_0^{1-\alpha-\gamma}} \left( \|p_0\|_{L^2(\Omega)} + \|\hat{f}(z)\|_{(\mathcal{N}_e; L^2(\Omega))} \right) e^{\mu\Lambda t_0} \left( \varepsilon + \frac{\varepsilon_N(\varrho)}{1-\varepsilon_N(\varrho)} \right),$$

where  $0 < d < \min\{\tilde{\alpha}, \pi/2 - \tilde{\alpha} - \delta'\}$ ,  $Q$  is given in Lemma 4.2.

Note that there exists  $\varrho \in (0, 1)$  such that  $e^{\mu\Lambda t_0} = (\varepsilon_N(\varrho))^{\varrho-1}$ . For fixed  $\alpha, \Lambda$  and  $\delta'$ , the optimal parameter  $\varrho^* \in (0, 1)$  can be determined by minimizing the convex function

$$(4.11) \quad \epsilon \cdot (\varepsilon_N(\varrho))^{\varrho-1} + (\varepsilon_N(\varrho))^\varrho.$$

In this study, we target high precision by setting  $\epsilon = 2.22 \times 10^{-16}$ , corresponding to the machine precision in IEEE double-precision arithmetic. Substituting  $\varrho^*$  into (4.9) yields the optimal parameters  $\mu^*$  and  $\tau^*$ , from which the convergence order of CIM can be established.

**Remark 4.4 (Spectral accuracy).** According to Theorem 3.4 in [43], for fixed  $\Lambda, \tilde{\alpha}$ , and  $\delta'$  satisfying  $0 < \tilde{\alpha}, \delta' < \pi/2$  and  $0 < \tilde{d} < \min\{\tilde{\alpha}, \pi/2 - \tilde{\alpha} - \delta'\}$ , if the parameters in (4.9) are chosen as optimal for the hyperbolic contour  $\Gamma$ , then the error satisfies  $E_N = \mathcal{O}(\varepsilon + e^{-CN})$  with  $C = \mathcal{O}(\frac{1}{\ln(\Lambda)})$ . This implies that the temporal semi-discrete CIM scheme (4.3) achieves spectral accuracy.

**4.2. Semi-discrete CLG.** In pursuit of spatio-temporal spectral accuracy, we adopt a spatial semi-discretization scheme that offers high precision while maintaining low computational cost. To this end, the Chebyshev-Legendre Galerkin (CLG) method is employed in this section for the spatial semi-discretization of both one- and two-dimensional formulations of Problem (1.6). The computational domain is set as  $\Omega = (-1, 1)^n$  for  $n = 1, 2$ .

**4.2.1. Exploring Chebyshev-Legendre Galerkin method.** Let  $(u, v) := \int_{\Omega} uv \, dr$  denote the inner product on  $\Omega$ , and  $\|u\|_{L^2(\Omega)} := (u, u)^{1/2}$  the corresponding norm. The variational formulation of Problem (1.6) is to find  $p(t, r) \in H_0^1(\Omega)$  such that for all  $v(t, r) \in (0, T] \times H_0^1(\Omega)$  and  $t \in (0, T]$ ,

$$(4.12) \quad \begin{aligned} & {}_0^{RL}\mathfrak{J}_t^{1-\gamma} \left( 1 + a {}_0^{RL}\mathfrak{D}_t^{\alpha} + \sum_{k=1}^K a_k {}_0^{RL}\mathfrak{D}_t^{\alpha_k} \right) (\partial_t p(t, r), v(t, r)) \\ & = - \left( 1 + b {}_0^{RL}\mathfrak{D}_t^{\beta} + \sum_{j=1}^J b_j {}_0^{RL}\mathfrak{D}_t^{\beta_j} \right) (\partial_r p(t, r), \partial_r v(t, r)) + (f(t, r), v(t, r)). \end{aligned}$$

We now construct an approximate solution to the variational form (4.12). To this end, we define the approximation space as follows.

Let  $\mathbb{P}_M(\Omega)$  be the space of all algebraic polynomials of degree at most  $M$  defined on  $\Omega$ , and define the approximation space as

$$(4.13) \quad \mathbb{V}_M^n = \mathbb{P}_M(\Omega) \cap H_0^1(\Omega), \quad \text{for } n = 1, 2, 3.$$

Then the semi-discrete scheme for Problem (1.6), termed the Chebyshev-Legendre Galerkin (CLG) method, is formulated as follows: find  $p_M \in \mathbb{V}_M^n$  such that for all  $v_M \in \mathbb{V}_M^n$ ,

$$(4.14) \quad \left\{ \begin{aligned} & {}_0^{RL}\mathfrak{J}_t^{1-\gamma} \left( 1 + a {}_0^{RL}\mathfrak{D}_t^{\alpha} + \sum_{k=1}^K a_k {}_0^{RL}\mathfrak{D}_t^{\alpha_k} \right) (\partial_t p_M, v_M) \\ & = - \left( 1 + b {}_0^{RL}\mathfrak{D}_t^{\beta} + \sum_{j=1}^J b_j {}_0^{RL}\mathfrak{D}_t^{\beta_j} \right) (\partial_r p_M, \partial_r v_M) + (I_M^c f, v_M), \quad t > 0, \\ & (p_M^0, v_M) = (I_M^c p_0, v_M), \quad t = 0. \end{aligned} \right.$$

Here,  $I_M^c : C(\bar{\Omega}) \rightarrow \mathbb{P}_M(\Omega)$  denotes the Chebyshev interpolation operator, defined by the interpolation condition  $I_M^c v(\xi_j) = v(\xi_j)$  at the Chebyshev-Gauss-Lobatto (CGL) points  $\xi_j := \cos\left(\frac{(2j+1)\pi}{2n+2}\right)$  for  $0 \leq j \leq M$ . The approximate solution is expressed as  $p_M = \sum_{k=0}^{M-2} p_k(t) \phi_k$ , with  $\phi_k$  being the basis of the approximation space  $\mathbb{V}_M^n$ .

The primary distinction between the CLG and the Legendre-Galerkin method lies in the use of the Chebyshev interpolation operator  $I_M^c$  in the terms  $(I_M^c f, v_M)$  and  $(I_M^c p_0, v_M)$ , as opposed to a Legendre interpolation operator. The CLG method combines the advantages of both the Legendre-Galerkin method (LG, which yields symmetric sparse matrices) and Chebyshev-Galerkin method (CG, which discrete Chebyshev transforms can be computed in  $\mathcal{O}(M \log_2 M)$  operations via the Fast Fourier Transform (FFT)). This hybrid strategy preserves the computational efficiency of Chebyshev methods, facilitated by the fast Legendre

transform, while maintaining the numerical stability characteristic of Legendre-based discretizations (see, e.g., [45, 46, 62, 63, 71]).

The computational efficiency of the CLG scheme relies heavily on a well-chosen basis for  $\mathbb{V}_M^n$  to simplify the structure of the resulting linear systems. The selection of basis functions and the algorithm implementation are tailored to the problem dimension, which we classify into one- and two-dimensional cases.

**4.2.2. Efficient 1D numerical implementation.** To facilitate the selection of basis functions adapted to the spatial dimension, we adopt the following convention: in one dimension,  $x = r \in \Omega = (-1, 1)$ ; in two dimensions,  $(x, y) = r \in \Omega = (-1, 1)^2$ , and similarly for higher dimensions. Following [46, 61, 63], we employ Lagrangian interpolation bases in the context of collocation and spectral element methods. Accordingly, for the one-dimensional case, we define the approximation space  $\mathbb{V}_M^1$  and choose a basis  $\{\phi_1(x), \phi_2(x), \dots, \phi_M(x)\}$ , where for  $\ell = 0, 1, 2, \dots, M-2$ ,  $\phi_\ell(x) = c_\ell(L_\ell(x) - L_{\ell-2}(x))$ . Here,  $L_\ell(x)$  denotes the Legendre polynomial of degree  $\ell$ , and the normalization constant is given by  $c_\ell = 1/\sqrt{4\ell+6}$ . The dimension of  $\mathbb{V}_M^1$  is  $M-1$ , consistent with the number of basis functions after imposing homogeneous Dirichlet boundary conditions.

Define the stiffness and mass matrix entries as  $a_{j\ell} := (\phi'_j(x), \phi'_\ell(x))$ ,  $m_{j\ell} := (\phi_j(x), \phi_\ell(x))$ , where the prime denotes the first derivative with respect to  $x$ . Since  $L_\ell(\pm 1) = (\pm 1)^\ell$ , the functions  $\{\phi_\ell(x)\}_{\ell=0}^{M-2}$  are linearly independent. Note that, using integration by parts yields

$$(4.15) \quad a_{j\ell} := (\phi'_j(x), \phi'_\ell(x)) = -(\phi''_j(x), \phi_\ell(x)) = -(\phi_j(x), \phi''_\ell(x)),$$

Using the orthogonality of Legendre polynomials in  $L^2(\Omega)$ ,

$$(4.16) \quad (L_j(x), L_\ell(x)) = \int_{-1}^1 L_j(x) L_\ell(x) dx = \frac{2}{2j+1} \delta_{j\ell}, \quad \forall j, \ell \geq 0,$$

and the recurrence relation  $(2\ell+1)L_\ell(x) = L'_{\ell+1}(x) - L'_{\ell-1}(x)$ , we the following explicit expressions

$$(4.17) \quad a_{j\ell} = \begin{cases} 1, & \ell = j, \\ 0, & \ell \neq j, \end{cases} \quad m_{j\ell} = m_{\ell j} = \begin{cases} c_\ell c_j \left( \frac{2}{2\ell+1} + \frac{2}{2\ell+5} \right), & \ell = j, \\ -c_\ell c_j \frac{2}{2\ell+1}, & \ell = j+2, \\ 0, & \text{Otherwise.} \end{cases}$$

Now, taking the test functions  $v_M = \phi_\ell(x)$  for  $\ell = 0, 1, \dots, M-2$ , the semi-discrete scheme (4.14) in one dimension becomes

$$(4.18) \quad \begin{cases} {}_0^{RL}\mathfrak{I}_t^{1-\gamma} \left( 1 + a {}_0^{RL}\mathfrak{D}_t^\alpha + \sum_{k=1}^K a_k {}_0^{RL}\mathfrak{D}_t^{\alpha_k} \right) (\partial_t p_M(t), \phi_\ell) \\ = - \left( 1 + b {}_0^{RL}\mathfrak{D}_t^\beta + \sum_{j=1}^J b_j {}_0^{RL}\mathfrak{D}_t^{\beta_j} \right) (p'_M(t), \phi'_\ell) + (I_M^c f(t), \phi_\ell), \quad t > 0, \\ (p_M^0, \phi_\ell) = (I_M^c p_0, \phi_\ell), \quad t = 0. \end{cases}$$

Applying the Laplace transform to (4.18) for all  $z \in \Sigma_{\theta,\delta}$ , we obtain

$$(4.19) \quad \begin{aligned} & z^\gamma \left( 1 + az^\alpha + \sum_{k=1}^K a_k z^{\alpha_k} \right) (\hat{p}_M(z), \phi_\ell) + \left( 1 + bz^\beta + \sum_{j=1}^J b_j z^{\beta_j} \right) (\hat{p}'_M(z), \phi'_\ell) \\ & = z^{\gamma-1} \left( 1 + az^\alpha + \sum_{k=1}^K a_k z^{\alpha_k} \right) (I_M^c p_0(z), \phi_\ell) + (I_M^c \hat{f}(z), \phi_\ell), \quad \ell = 0, 1, \dots, M-2. \end{aligned}$$

Define  $p_\ell^0 = (I_M^c p_0, \phi_\ell)$ , and let  $\mathbf{p}_0 = (p_0^0, p_1^0, \dots, p_{M-2}^0)^T$ . Similarly, define  $\hat{f}_\ell = (I_M^c \hat{f}(z), \phi_\ell)$  and  $\hat{\mathbf{f}} = (\hat{f}_0, \hat{f}_1, \dots, \hat{f}_{M-2})^T$ . Expanding the solution as  $\hat{p}_M = \sum_{\ell=0}^{M-2} \hat{p}_\ell(z) \phi_\ell$ , we define the coefficient vector  $\hat{\mathbf{p}} = (\hat{p}_0(z), \hat{p}_1(z), \dots, \hat{p}_{M-2}(z))^T$ . From the previous analysis, the stiffness matrix  $\mathbf{A} = (a_{j\ell})_{0 \leq j, \ell \leq M-2}$  is identical to the identity matrix  $\mathbf{I}$ , while the mass matrix  $\mathbf{M} = (m_{j\ell})_{0 \leq j, \ell \leq M-2}$  is pentadiagonal. Thus, the scheme (4.18) is equivalent to the following matrix equation in the Laplace domain

$$(4.20) \quad \begin{aligned} & \left[ \left( z^\gamma + az^{\alpha+\gamma} + \sum_{k=1}^K a_k z^{\alpha_k+\gamma} \right) \mathbf{M} + \left( 1 + bz^\beta + \sum_{j=1}^J b_j z^{\beta_j} \right) \mathbf{A} \right] \hat{\mathbf{p}} \\ & = \left( z^{\gamma-1} + az^{\alpha+\gamma-1} + \sum_{k=1}^K a_k z^{\alpha_k+\gamma-1} \right) \mathbf{p}_0 + \hat{\mathbf{f}}, \quad \forall z \in \Sigma_{\theta,\delta}. \end{aligned}$$

The resulting system matrix is pentadiagonal, which facilitates the use of efficient algorithms for solving the corresponding linear equations.

**4.2.3. Efficient 2D numerical implementation.** For the two-dimensional case, building upon the one-dimensional formulation, the approximation space is naturally constructed as

$$(4.21) \quad \mathbb{V}_M^2 = \left\{ \phi_j(x) \phi_\ell(y), \quad j, \ell = 0, 1, \dots, M-2 \right\}.$$

Choosing test functions of the form  $v_M = \phi_j(x) \phi_\ell(y)$  for  $j, \ell = 0, 1, \dots, M-2$ , the semi-discrete scheme (4.14) for the two-dimensional problem becomes

$$(4.22) \quad \begin{cases} {}_0^{RL} \mathfrak{I}_t^{1-\gamma} \left( 1 + a {}_0^{RL} \mathfrak{D}_t^\alpha + \sum_{k=1}^K a_k {}_0^{RL} \mathfrak{D}_t^{\alpha_k} \right) (\partial_t p_M(t), \phi_j \phi_\ell) \\ \quad + \left( 1 + b {}_0^{RL} \mathfrak{D}_t^\beta + \sum_{j=1}^J b_j {}_0^{RL} \mathfrak{D}_t^{\beta_j} \right) [(p'_M(t), \phi'_j \phi_\ell) + (p'_M, \phi_j \phi'_\ell)] = (I_M^c f(t), \phi_j \phi_\ell), \quad t > 0, \\ (P_M^0, \phi_j \phi_\ell) = (I_M^c p_0, \phi_j \phi_\ell), \quad t = 0. \end{cases}$$

Applying the Laplace transform, for  $j, \ell = 0, 1, \dots, M-2$ , we obtain

$$(4.23) \quad \begin{aligned} & z^\gamma \left( 1 + az^\alpha + \sum_{k=1}^K a_k z^{\alpha_k} \right) (\hat{p}_M(z), \phi_j \phi_\ell) + \left( 1 + bz^\beta + \sum_{j=1}^J b_j z^{\beta_j} \right) (\hat{p}'_M(z), \phi'_j \phi_\ell + \phi_j \phi'_\ell) \\ & = z^{\gamma-1} \left( 1 + az^\alpha + \sum_{k=1}^K a_k z^{\alpha_k} \right) (I_M^c p_0(z), \phi_j \phi_\ell) + (I_M^c \hat{f}(z), \phi_j \phi_\ell), \quad \forall z \in \Sigma_{\theta,\delta}. \end{aligned}$$

To distinguish from the one-dimensional case, we denote the corresponding quantities using uppercase letters. Define  $P_{j,\ell}^0 = (I_M^c p_0, \phi_j \phi_\ell)$ ,  $\mathbf{P}_0 = (P_{j,\ell}^0)_{0 \leq j, \ell \leq M-2}$ ,  $\hat{f}_{j,\ell} = (I_M^c \hat{f}, \phi_j \phi_\ell)$ ,  $\hat{\mathbf{F}} = (\hat{f}_{j,\ell})_{0 \leq j, \ell \leq M-2}$ . Expanding the solution as  $\hat{P}_M = \sum_{j,\ell=0}^{M-2} \hat{P}_{j,\ell}(z) \phi_j \phi_\ell$ ,  $\hat{\mathbf{P}} = (\hat{P}_{j,\ell}(z))_{0 \leq j, \ell \leq M-2}$ , the matrix form of equation (4.22) in the Laplace domain is given by

$$(4.24) \quad \begin{aligned} & z^\gamma \left( 1 + az^\alpha + \sum_{k=1}^K a_k z^{\alpha_k} \right) \hat{\mathbf{P}} \hat{\mathbf{M}} + \left( 1 + bz^\beta + \sum_{j=1}^J b_j z^{\beta_j} \right) (\hat{\mathbf{M}} \hat{\mathbf{P}} \mathbf{A}^T + \mathbf{A} \hat{\mathbf{P}} \mathbf{M}) \\ & = z^{\gamma-1} \left( 1 + az^\alpha + \sum_{k=1}^K a_k z^{\alpha_k} \right) \mathbf{P}_0 + \hat{\mathbf{F}}, \quad \forall z \in \Sigma_{\theta,\delta}. \end{aligned}$$

Since  $\mathbf{A} = \mathbf{I}$ , the equation can be rewritten using Kronecker products as

$$(4.25) \quad \begin{aligned} & \left[ z^\gamma \left( 1 + az^\alpha + \sum_{k=1}^K a_k z^{\alpha_k} \right) \mathbf{M} \otimes \mathbf{M} + \left( 1 + bz^\beta + \sum_{j=1}^J b_j z^{\beta_j} \right) (\mathbf{M} \otimes \mathbf{I} + \mathbf{I} \otimes \mathbf{M}) \right] \hat{\mathbf{P}} \\ & = z^{\gamma-1} \left( 1 + az^\alpha + \sum_{k=1}^K a_k z^{\alpha_k} \right) \mathbf{P}_0 + \hat{\mathbf{F}}, \quad \forall z \in \Sigma_{\theta,\delta}. \end{aligned}$$

**4.3. Stability and convergence of the CLG method.** Having introduced the CLG scheme (4.14), we now establish its stability and convergence, which are essential for ensuring its reliability and effectiveness. Our analysis begins with the one-dimensional semi-discrete scheme (4.14); the results and proofs can be directly extended to higher dimensions.

In the spatial semi-discrete scheme (4.14), the initial data and source term are numerically approximated rather than analytically evaluated. It is therefore necessary to investigate the stability of the scheme under such approximations. To facilitate this analysis, we introduce several projection operators and recall their fundamental approximation properties.

We begin by defining the  $L^2$  orthogonal projection operator  $P_M^L : L^2(\Omega) \rightarrow \mathbb{P}_M$ , requiring that for all  $v_h \in \mathbb{P}_M$  and  $u \in L^2(\Omega)$ ,  $(P_M^L u, v_h) = (u, v_h)$ . This projection satisfies the following approximation estimate.

**Lemma 4.5 (see [63]).** *If  $u \in H^{\tilde{r}}(\Omega)$  with  $\tilde{r} \in \mathbb{N}$ , then there exists a positive constant  $C$  such that*

$$(4.26) \quad \|P_M^L u - u\|_{H^l(\Omega)} \leq CM^{l-\tilde{r}} \|u\|_{H^{\tilde{r}}(\Omega)}, \quad \text{for } 0 \leq l \leq \tilde{r}.$$

Next, we introduce the  $H_0^1$ -orthogonal projection  $\Pi_M : H_0^1(\Omega) \rightarrow \mathbb{P}_M$ , defined by  $\Pi_M u(x) := \int_{-1}^x P_{M-1}^L \frac{\partial}{\partial s} u(s) ds$ . By construction,  $\Pi_M$  satisfies  $((\Pi_M u(x))', v') = (u', v')$  for all  $v \in \mathbb{P}_M$ . The operator  $\Pi_M$  also admits the following estimate.

**Lemma 4.6 (see [70]).** *If  $u \in H^{\tilde{r}}(\Omega) \cap H_0^1(\Omega)$  with  $\tilde{r} \geq 1$ , then there exists a positive constant  $C$  such that*

$$(4.27) \quad \|\Pi_M u - u\|_{H^l(\Omega)} \leq CM^{l-\tilde{r}} \|u\|_{H^{\tilde{r}}(\Omega)}, \quad \text{for } -1 \leq l \leq 1.$$

Finally, we consider the Chebyshev interpolation operator  $I_M^c(\Omega) : C(\bar{\Omega}) \rightarrow \mathbb{S}_M$  (see [63]), defined by  $I_M^c u(\xi_j) = u(\xi_j)$ , where  $\xi_j = \cos(\frac{\pi j}{M})$ ,  $0 \leq j \leq M$ , are the Chebyshev points. This operator exhibits the following approximation property.

**Lemma 4.7** (see [36, 46, 70, 71]). *Let  $u \in H^1(\Omega)$ . There exists a constant  $C > 0$  such that*

$$(4.28) \quad M\|I_M^c u - u\|_{L^2(\Omega)} + \|I_M^c u\|_{H^1(\Omega)} \leq C\|u\|_{H^1(\Omega)}.$$

Moreover, if  $u \in H^{\tilde{r}}(\Omega)$  with  $\tilde{r} \geq 1$ , then

$$(4.29) \quad \|I_M^c u - u\|_{H^l(\Omega)} \leq CM^{l-\tilde{r}}\|u\|_{H^{\tilde{r}}(\Omega)}, \quad \text{for } 0 \leq l \leq 1.$$

Let  $p_M$ ,  $p_0$ , and  $f$  be computed via (4.14), with corresponding numerical errors denoted by  $\tilde{p}$ ,  $\tilde{p}_0$ , and  $\tilde{f}$ , respectively. Based on the preceding analysis, for any test function  $v_M \in \mathbb{V}_M^1 = \mathbb{P}_M(\Omega) \cap H_0^1(\Omega)$ , the following identity holds

$$(4.30) \quad \begin{aligned} & {}_0^{RL}\mathfrak{I}_t^{1-\gamma} \left( 1 + a {}_0^{RL}\mathfrak{D}_t^\alpha + \sum_{k=1}^K a_k {}_0^{RL}\mathfrak{D}_t^{\alpha_k} \right) (\partial_t(p_M(t) + \tilde{p}), v_M) \\ &= - \left( 1 + b {}_0^{RL}\mathfrak{D}_t^\beta + \sum_{j=1}^J b_j {}_0^{RL}\mathfrak{D}_t^{\beta_j} \right) (p'_M(t) + \tilde{p}', v'_M) + (I_M^c f(t) + \tilde{f}, v_M), \quad t > 0. \end{aligned}$$

From this, one may directly verify that the errors  $\tilde{p}$ ,  $\tilde{p}_0$ , and  $\tilde{f}$  satisfy the following error equation

$$(4.31) \quad \begin{aligned} & {}_0^{RL}\mathfrak{I}_t^{1-\gamma} \left( 1 + a {}_0^{RL}\mathfrak{D}_t^\alpha + \sum_{k=1}^K a_k {}_0^{RL}\mathfrak{D}_t^{\alpha_k} \right) (\partial_t \tilde{p}, v_M) \\ &= - \left( 1 + b {}_0^{RL}\mathfrak{D}_t^\beta + \sum_{j=1}^J b_j {}_0^{RL}\mathfrak{D}_t^{\beta_j} \right) (\tilde{p}', v'_M) + (\tilde{f}, v_M), \quad t > 0. \end{aligned}$$

By the arbitrariness of the test function, together with the application of the Laplace transform, we obtain

$$(4.32) \quad \widehat{\tilde{p}}(z) = \mathcal{H}(z)\tilde{p}_0 + \left( z^{\gamma-1} + az^{\alpha+\gamma-1} + \sum_{k=1}^K a_k z^{\alpha_k+\gamma-1} \right)^{-1} \mathcal{H}(z)\widehat{\tilde{f}}(z), \quad z \in \Sigma_{\theta, \delta}.$$

where the operator  $\mathcal{H}(z)$  is defined by (3.2). This identity provides the foundation for the subsequent stability analysis.

**Theorem 4.8 ( $L^2$ -stability).** *Suppose that  $p_M$ ,  $p_0$ , and  $f$  are computed via (4.14), with corresponding errors  $\tilde{p}$ ,  $\tilde{p}_0$ , and  $\tilde{f}$ , respectively. Then there exist a positive constants  $C$ , independent of  $M$  and  $t$ , such that for all  $t \in (0, T]$  the following estimates hold,*

$$(4.33) \quad \|\tilde{p}(t)\|_{L^2(\Omega)} \leq C_1 \left( \|\tilde{p}_0\|_{L^2(\Omega)} + t^{\alpha+\gamma-1} \|\widehat{\tilde{f}}(z)\|_{(\mathcal{N}_e; L^2(\Omega))} \right).$$

*Proof.* By combining (4.32) with the analytical technique of Thm. 3.5 and the properties of the operator  $\mathcal{H}(z)$  from Lemma 3.2, we obtain the estimate

$$\begin{aligned} \|\tilde{p}(t)\|_{L^2(\Omega)} &\leq C \int_{\Gamma_{\theta,\delta}} e^{|z|t \cos(\theta)} \|\mathcal{H}(z)\|_{L^2(\Omega) \rightarrow L^2(\Omega)} \|\tilde{p}_0\|_{L^2(\Omega)} |dz| \\ &\quad + C \int_{\Gamma_{\theta,\delta}} e^{|z|t \cos(\theta)} \|g(z)\mathcal{H}(z)\|_{L^2(\Omega) \rightarrow L^2(\Omega)} \|\widehat{\tilde{f}}(z)\|_{L^2(\Omega)} |dz| \\ &\leq C \int_{\Gamma_{\theta,\delta}} e^{|z|t \cos(\theta)} |z|^{-1} |dz| \|\tilde{p}_0\|_{L^2(\Omega)} + C \int_{\Gamma_{\theta,\delta}} e^{|z|t \cos(\theta)} |z|^{-(\alpha+\gamma)} \|\widehat{\tilde{f}}(z)\|_{L^2(\Omega)} |dz| \\ &\leq C \|\tilde{p}_0\|_{L^2(\Omega)} + C t^{\alpha+\gamma-1} \|\widehat{\tilde{f}}(z)\|_{(\mathcal{N}_e; L^2(\Omega))}. \end{aligned}$$

This completes the proof.  $\blacksquare$

Theorem 4.8 establishes the unconditional stability of the CLG method in the  $L^2$ -norm. We now proceed to its convergence analysis. Let  $p(t)$  be the solution to Problem (1.6) governed by (4.12), and let  $p_M(t)$  be its numerical approximation defined in (4.18). Introduce the comparison function  $p^*(t) = \Pi_M p(t)$  and define the error  $\omega(t) = p^*(t) - p_M(t)$ . The following convergence results are then established with respect to the CLG scheme.

**Theorem 4.9 ( $L^2$ -Convergence).** *Let  $p(t)$  be the solution of Problem (1.6), and let  $p_M(t)$  be its numerical approximation defined in (4.18). Then there exists some positive constants  $C_i$  ( $i = 1, 2$ ), independent of  $M$  and  $t$ , such that the following error estimates hold for all  $t \in (0, T]$ :*

(i) *For  $f \equiv 0$ , if  $u_0 \in H^{\tilde{r}}(\Omega)$  with  $\tilde{r} \geq 1$ , then*

$$(4.34) \quad \|p(t) - p_M(t)\|_{L^2(\Omega)} \leq C_1 M^{-\tilde{r}} \|p_0\|_{H^{\tilde{r}}(\Omega)}.$$

(ii) *For  $p_0 \equiv 0$ , if  $\|\widehat{f}(z)\|_{(\mathcal{N}_e; H^{\tilde{r}}(\Omega))} < \infty$  with  $\tilde{r} \geq 1$ , then*

$$(4.35) \quad \|p(t) - p_M(t)\|_{L^2(\Omega)} \leq C_2 M^{-\tilde{r}} t^{(\alpha+\gamma)-1} \|\widehat{f}(z)\|_{(\mathcal{N}_e; H^{\tilde{r}}(\Omega))}.$$

*Proof.* For case (i), with  $f \equiv 0$ , and  $t \in (0, T]$ , we decompose the error  $p(t) - p_M(t)$  as

$$(4.36) \quad p(t) - p_M(t) = (p(t) - p^*(t)) + (p^*(t) - p_M(t)) := \rho(t) + \omega(t),$$

which implies  $\|p(t) - p_M(t)\|_{L^2(\Omega)} \leq \|\rho(t)\|_{L^2(\Omega)} + \|\omega(t)\|_{L^2(\Omega)}$ . We proceed to estimate each term separately. For  $\|\rho(t)\|_{L^2(\Omega)}$ , applying Lemma 4.6 and the regularity results from Thm. 3.5 (or Corollary 3.7) yields

$$(4.37) \quad \|\rho(t)\|_{L^2(\Omega)} = \|\Pi_M p(t) - p(t)\|_{L^2(\Omega)} \leq C M^{l-\tilde{r}} \|p(t)\|_{\dot{H}^{\tilde{r}}(\Omega)} \leq C M^{l-\tilde{r}} \|p_0\|_{\dot{H}^{\tilde{r}}(\Omega)}.$$

To bound  $\omega(t)$ , we employ (4.12) and (4.18). Taking the Laplace transform, we establish that for all  $\phi \in H_0^1(\Omega)$  and  $z \in \Sigma_{\theta,\delta}$

$$\begin{aligned} &z^\gamma \left( 1 + az^\alpha + \sum_{k=1}^K a_k z^{\alpha_k} \right) (\widehat{\omega}(z), \phi) + \left( 1 + bz^\beta + \sum_{j=1}^J b_j z^{\beta_j} \right) (\widehat{\omega}'(z), \phi') \\ &= z^{\gamma-1} \left( 1 + az^\alpha + \sum_{k=1}^K a_k z^{\alpha_k} \right) (\Pi_M p_0 - p_0 + p_0 - I_M^C p_0, \phi). \end{aligned}$$

This implies

$$\widehat{\omega}(z) = \mathcal{H}(z) \left( \Pi_M p_0 - p_0 + p_0 - I_M^C p_0 \right), \quad z \in \Sigma_{\theta, \delta},$$

where  $\mathcal{H}(z)$  is defined in Lemma 3.2. Applying Lemmas 3.2, 4.6 and 4.7, we deduce

$$\begin{aligned} (4.38) \quad \|\omega(t)\|_{L^2(\Omega)} &\leq C \int_{\Gamma_{\theta, \delta}} e^{t|z| \cos(\theta)} |z|^{-1} |dz| \left( \|\Pi_M p_0 - p_0\|_{L^2(\Omega)} + \|p_0 - I_M^C p_0\|_{L^2(\Omega)} \right) \\ &\leq C M^{-\tilde{r}} \|p_0\|_{H^{\tilde{r}}(\Omega)}. \end{aligned}$$

Combining (4.37) and (4.38) completes the proof of Thm. 4.9(i).

For case (ii), following a similar approach to Thm. 4.9 (i) and leveraging the regularity results from Thm. 3.6 and Corollary 3.7, we first estimate

$$(4.39) \quad \|\rho(t)\|_{L^2(\Omega)} = \|\Pi_M p(t) - p(t)\|_{L^2(\Omega)} \leq C M^{-\tilde{r}} \|p(t)\|_{\dot{H}^{\tilde{r}}(\Omega)} \leq C t^{\alpha+\gamma-1} M^{-\tilde{r}} \|\widehat{f}(z)\|_{(\mathcal{N}_e; \dot{H}^{\tilde{r}}(\Omega))}.$$

For  $\omega(t)$ , we have

$$\widehat{\omega}(z) = g(z) \mathcal{H}(z) \left( \Pi_M \widehat{f}(z) - \widehat{f}(z) + \widehat{f}(z) - I_M^C \widehat{f}(z) \right), \quad z \in \Sigma_{\theta, \delta},$$

where  $g(z)$  is defined in Lemma 3.2. Applying Lemmas 4.6 and 4.7 yields

$$\begin{aligned} (4.40) \quad \|\omega(t)\|_{L^2(\Omega)} &\leq C M^{-\tilde{r}} \int_{\Gamma_{\theta, \delta}} e^{|z| \cos \theta t} |z|^{-(\alpha+\gamma)} \|\widehat{f}\|_{H^{\tilde{r}}(\Omega)} |dz| \\ &\leq C M^{-\tilde{r}} t^{(\alpha+\gamma)-1} \|\widehat{f}(z)\|_{(\mathcal{N}_e; H^{\tilde{r}}(\Omega))}, \end{aligned}$$

Combining the estimates (4.39) and (4.40) completes the proof of Thm. 4.9(ii).  $\blacksquare$

For the stability and convergence analysis of spectral methods, the commonly used approach often relies on establishing connections between the solution of the equation and Gronwall's inequality to derive relevant estimates. However, in the case of the MT-TFJE considered here, both the construction of such inequalities and the implementation of related techniques present notable challenges. In this section, the analytical approach we provide is based on the perspective of the traditional Galerkin finite element method, conducting the analysis in the Laplace space. This methodology not only tightly couples the solution theory with the stability and convergence analysis of the numerical scheme but also introduces novel proof techniques, thereby underscoring the coherence and systematic structure of the present study.

**4.4. The CIM-CLG algorithm.** The fully discrete scheme is constructed by applying the CIM to the semi-discrete scheme CLG given in (4.20) for the one-dimensional case and (4.25) for the two-dimensional case. Specifically, the numerical solution is computed via

$$(4.41) \quad p_M^N(t, r) = \frac{\tau}{\pi} \operatorname{Im} \left\{ \sum_{k=0}^{N-1} e^{z_k t} \cdot \widehat{\mathbf{p}} \cdot z'_k \right\},$$

where  $\widehat{\mathbf{p}} = [\widehat{p}_0(z_k), \widehat{p}_1(z_k), \dots, \widehat{p}_{M-2}(z_k)]^T$  denotes the solution vector approximated at the quadrature points  $z_k = (k + \frac{1}{2})\tau$  and  $k = 0, 1, 2, \dots, N-1$ . Each vector  $\widehat{\mathbf{p}}$  is obtained by solving

the corresponding linear system (i.e., (4.20) in one dimension and (4.25) in two dimensions) in the Laplace domain. Owing to the strict diagonal dominance of the coefficient matrices, each such system admits a unique solution.

On the basis of Theorems 4.3 and 4.9, we now establish the following error estimate for the fully discrete scheme.

**Theorem 4.10 (Convergence).** *Let  $p(t, r)$  be the solutions of Problem (1.6), and let  $p_M^N(r, t)$  be its approximation defined as in (4.41). For  $0 < t_0 \leq t \leq \Lambda t_0$  and  $M > 0$ , the following estimates hold:*

(i) *Suppose  $f \equiv 0$ . If  $p_0 \in \dot{H}^{\tilde{r}}(\Omega)$  with  $\tilde{r} \geq 1$ , then there exists a constant  $C > 0$  such that*

$$\|p(t, r) - p_M^N(t)\|_{L^2(\Omega)} \leq CQ \Xi e^{\mu \Lambda t_0} \left( (1 - \varrho) \cdot \varepsilon + \frac{\varrho \cdot \varepsilon_N(\varrho)}{1 - \varepsilon_N(\varrho)} + M^{-\tilde{r}} \right) \|p_0\|_{\dot{H}^{\tilde{r}}(\Omega)}.$$

(ii) *Suppose  $p_0 \equiv 0$ . If  $f \in L^1(0, T; \dot{H}^{\tilde{r}}(\Omega))$  with  $\tilde{r} \geq 1$ , then there exists a constant  $C > 0$  such that*

$$\|p(t, r) - p_M^N(t)\|_{L^2(\Omega)} \leq CQ \Xi e^{\mu \Lambda t_0} \left( (1 - \varrho) \cdot \varepsilon + \frac{\varrho \cdot \varepsilon_N(\varrho)}{1 - \varepsilon_N(\varrho)} + t^{(\alpha+\gamma)-1} M^{-\tilde{r}} \right) \|f\|_{(N_e; \dot{H}^{\tilde{r}}(\Omega))}.$$

Here,  $Q$  is defined in Prop. 4.2,  $\Xi := \frac{L((1-\nu)\mu t_0 \sin(\tilde{\alpha}-d))}{t_0^{1-\alpha-\gamma}}$ , and  $\varrho, \nu \in (0, 1)$  are arbitrary.

Guided by the design principles of the fully discrete scheme, the specific algorithm is implemented as shown in Algorithm 4.1. This algorithm is referred to as the CIM-CLG.

**5. Numerical experiments.** This section presents several numerical experiments conducted to validate our theoretical findings and demonstrate the high numerical performance of the CIM-CLG algorithm.

To quantitatively evaluate the accuracy of the method, we introduce the following error measures. When the exact solution  $p(t)$  is available, we define the temporal error  $error_N$  as a function of the time discretization parameter  $N$ , and the spatial error  $error_M$  as a function of the polynomial degree  $M$ , respectively,

$$error_N(N) = \max_{t_0 \leq t \leq \Lambda t_0} \|p(t) - p_M^N(t)\|_{L^2(\Omega)}, \quad error_M(M) = \|p(t) - p_M^N(t)\|_{L^2(\Omega)}$$

with fixed  $M$  or  $N$ . The corresponding orders of convergence in space and time are defined as

$$Order_s = \frac{\ln(error_M(M_j)/error_M(M_{j+1}))}{\ln(M_{j+1}/M_j)}, \quad Order_t = \frac{\ln(error_N(N_j)/error_N(N_{j+1}))}{\ln(N_{j+1}/N_j)},$$

where  $\{M_j\}$  and  $\{N_j\}$  are strictly increasing sequences of polynomial degrees and time discretization parameters, respectively. In cases where the exact solution is unknown, we employ the following error indicators

$$error_N(N) = \max_{t_0 \leq t \leq \Lambda t_0} \|p_M^{100}(t) - p_M^N(t)\|_{L^2(\Omega)}, \quad error_M(M) = \|p_{2M}^N(t) - P_M^N(t)\|_{L^2(\Omega)},$$

again with fixed  $M$  or  $N$ . The numerical convergence order is then estimated as

$$Order = \frac{\ln(error_{M/2}/error_M)}{\ln(2)},$$

**Algorithm 4.1** CIM-CLG algorithm

---

```

1: Input:  $\alpha, \alpha_k, \beta, \beta_j, \gamma, t_0, \Lambda \geq 1, T = \Lambda t_0, t, K, J, \tilde{\alpha}, \delta', \varepsilon = 2.22 \times 10^{-16}, N, M, D$ .
2: Output: The numerical result  $\mathbf{p}_M^N(r, t)$ .
3: while  $j < D$  do
4:    $\varrho_j \leftarrow 1/D \cdot j$ ;
5:    $a(\varrho_j) \leftarrow \cosh^{-1} \left( \frac{\Lambda}{(1-\varrho_j) \sin(\tilde{\alpha}-\tilde{d})} \right)$ ;
6:    $\varepsilon_N(\varrho_j) \leftarrow \exp \left( \frac{2\pi\tilde{d}N}{a(\varrho_j)} \right)$ ;
7:    $\varrho^* \leftarrow \min_j \left( (1 - \varrho_j) \cdot \varepsilon + \frac{\varrho_j \cdot \varepsilon_N(\varrho_j)}{1 - \varepsilon_N(\varrho_j)} \right)$ ;
8: end while
9: Substitute  $\varrho^*$  into (4.9) to get the optimal parameters  $\tau^*$  and  $\mu^*$ .
10: return  $\tau^*$  and  $\mu^*$ .
11: while  $k < N$  do
12:    $z_k \leftarrow \mu^* (1 + \sin(i(k + 1/2)\tau^* - \tilde{\alpha}))$ ,  $i^2 = -1$ ;
13:    $z'_k \leftarrow i\mu^* \cos(i(k + 1/2)\tau^* - \tilde{\alpha}))$ ,  $i^2 = -1$ ;
14:    $p_{0,j} \leftarrow$  Evaluate the Legendre coefficients of  $I_M^c p_0$  from  $\{p(0, r_j)\}_{j=0}^{M-2}$ ;
15:    $\hat{f}_j \leftarrow$  Evaluate the Legendre coefficients of  $I_M^c \hat{f}_j$  from  $\{\hat{f}(z, r_j)\}_{j=0}^{M-2}$ ;
16:    $\hat{\mathbf{p}}(z_k) \leftarrow$  Solve  $[(z^\gamma + az^{\alpha+\gamma} + \sum_{k=1}^K a_k z^{\alpha_k+\gamma}) \mathbf{M} + (1 + bz^\beta + \sum_{j=1}^J b_j z^{\beta_j}) \mathbf{A}] \hat{\mathbf{p}} = (z^{\gamma-1} + az^{\alpha+\gamma-1} + \sum_{k=1}^K a_k z^{\alpha_k+\gamma-1}) \mathbf{p}_0 + \hat{\mathbf{f}}$ ;
17:    $\hat{p}_M \leftarrow$  Evaluate  $\hat{p}_M = \sum_{j=0}^{M-2} \hat{p}_j \phi_i(x_j)$ ,  $j = 0, 1, \dots, M$ .
18: end while
19: return  $\hat{\mathbf{p}}(z_k)$ .
20:  $\mathbf{p}_M^N(t, r) \leftarrow \frac{\tau^*}{\pi} \text{Im} \left\{ \sum_{k=0}^{N-1} e^{z_k t} \cdot \hat{\mathbf{p}}(z_k) \cdot z'_k \right\}$ .

```

---

so that the numerical convergence behavior follows  $\mathcal{O}(M^{-\text{Order}})$ .

Analogous definitions and convergence orders apply when errors are measured in the  $L^\infty$ -norm. Furthermore, Based on Prop. 2.1, the MSD analysis in Sub. 2.1.1, and the result established in Lemma 3.2, we concluded that the dominant term in Problem (1.6) corresponds to the case  $K = J = 0$ . To streamline the numerical simulations, we set  $K = J = 0$  throughout all numerical examples. This choice is not merely a computational convenience; it is a physically and mathematically justified simplification that focuses the analysis on the dominant dynamics while preserving the fundamental structure of the problem.

In all numerical examples, the domain is taken as  $\Omega = (-1, 1)^d$  ( $d = 1, 2$ ). The contour parameters are set to  $\delta' = \pi/8$  and  $\tilde{\alpha} = \pi/4$ . The experiments are carried out in MATLAB R2025a on a PC with an Intel(R) Core(TM) i7-6700 CPU @3.40GHz and 16.00GB of RAM.

**5.1. Example 1. (A scalar problem).** To intuitively demonstrate the spectral accuracy and numerical stability of the CIM, we consider the following time fractional differential equation

$$(5.1) \quad {}_0^{RL}\mathfrak{I}_t^{1-\gamma} (1 + {}_0^{RL}\mathfrak{D}_t^\alpha) \partial_t p(t) + (1 + {}_0^{RL}\mathfrak{D}_t^\beta) \lambda p(t) = f(t),$$

with exact solution  $p(t) = 1 + t^{4/5}$  (which has limited temporal regularity), where  $\lambda \in \mathbb{R}_+$  is a specified positive constant. We set  $p_0 = 1$  accordingly, and the source term  $f$  is explicitly derived as

- $f(t) = \lambda \left( 1 + t^{4/5} + \frac{bt^{-\beta}}{\Gamma(1-\beta)} + \frac{b\Gamma(9/5)t^{5/4-\beta}}{\Gamma(9/5-\beta)} \right) + \frac{4}{5}\Gamma\left(\frac{4}{5}\right) \left( \frac{t^{5/4-\gamma}}{\Gamma(9/5-\gamma)} + \frac{at^{5/4-\alpha-\gamma}}{\Gamma(9/5-\alpha-\gamma)} \right).$

We employ the CIM for numerical discretization and quantify the absolute error as a function of the discretization parameter  $N$  via

$$\text{Error}(N) = \max_{t_0 \leq t \leq \Lambda t_0} |p(t) - p^N(t)|.$$

Figure 5.1(a) shows the convergence behavior of  $\text{Error}(N)$  for different values of  $\Lambda$ , demonstrating the spectral accuracy of the method. Figures 5.1(b) and (c) present a stability analysis under various fractional orders  $\alpha$ ,  $\beta$ , and  $\gamma$ , as well as different ratios  $b/a$ , further confirming the robustness of the CIM.

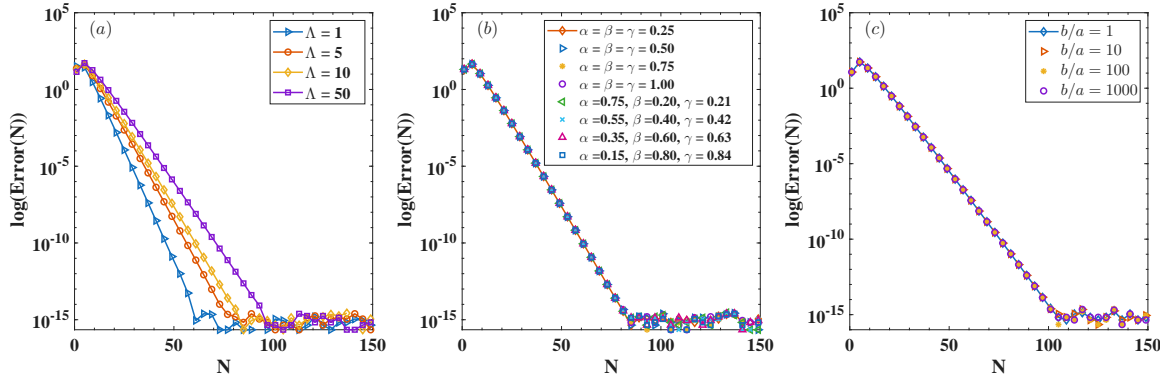


**Figure 5.1.** Numerical performance of the CIM illustrating its spectral accuracy, stability, and robustness. (a) Error evolution with the number of quadrature points  $N$  for various  $\Lambda$  (semi-discrete scheme (4.3)), with  $\alpha = 0.50$ ,  $\beta = 0.35$ ,  $\gamma = 0.45$ ,  $\lambda = 1.50$ ,  $a = 1.00$ ,  $b = 100.00$ , and  $t = 0.50$ . (b) Error under varying fractional orders, with  $a = 1.00$ ,  $b = 10.00$  and  $\Lambda = 10.00$ . (c) Error across different ratios of  $b/a$ , with  $\alpha = 0.50$ ,  $\beta = 0.35$ ,  $\gamma = 0.45$ ,  $\lambda = 1.50$ , and  $t = 0.50$ .

As demonstrated in Fig. 5.1, the proposed approach preserves the spectral accuracy and stability of the CIM across a wide range of fractional orders. These numerical findings are in full agreement with the theoretical predictions in Remark 4.4. Specifically, the CIM achieves a convergence rate of  $\mathcal{O}(\varepsilon + e^{-cN})$ , where  $c = \mathcal{O}(1/\ln(\Lambda))$ .

**5.2. Example 2. (1-D problem with known source).** In this example, we consider a scenario with zero initial data and a known source term. By comparing the exact solution with numerical results, we verify that the proposed scheme achieves spatio-temporal spectral accuracy.

Let the exact solution of problem (1.6) be  $p(t, x) = t^\kappa \sin(\pi x)$ , where  $\kappa \in \mathbb{R}_+$  with the corresponding source term given by

- $f(t) = \sin(\pi x) \left[ \Gamma(\kappa + 1) \left( \frac{t^{\kappa-\gamma}}{\Gamma(\kappa+1-\gamma)} + \frac{t^{\kappa-\alpha-\gamma}}{\Gamma(\kappa+1-\alpha-\gamma)} \right) + \pi^2 \left( t^\kappa + b \frac{t^{\kappa-\beta}}{\Gamma(\kappa+1-\beta)} \right) \right].$

Numerical results are presented in Figures 5.2 and 5.3, and Tables 1–2.

In both Figures 5.2 and 5.3, we set  $\kappa = \frac{1}{4}$ , which corresponds to the solution with limited temporal regularity. The numerical results demonstrate that the proposed CIM-CLG algorithm effectively solves the MT-TFJE even under conditions of low temporal regularity. As further shown in Tables 1 and 2, the algorithm achieves high convergence orders and maintains

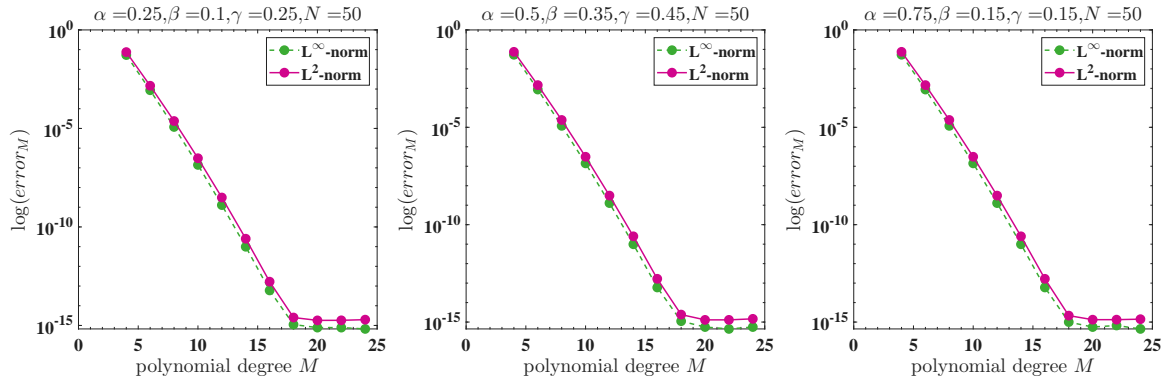


**Figure 5.2.** Spatial spectral accuracy convergence of the CLG method. The figure shows the exponential decay of spatial errors with increasing polynomial degree under different fractional orders, with given parameters  $a = 1$ ,  $b = 1000$ ,  $t = 0.5$ , and  $\kappa = 1/4$  (low temporal regularity).

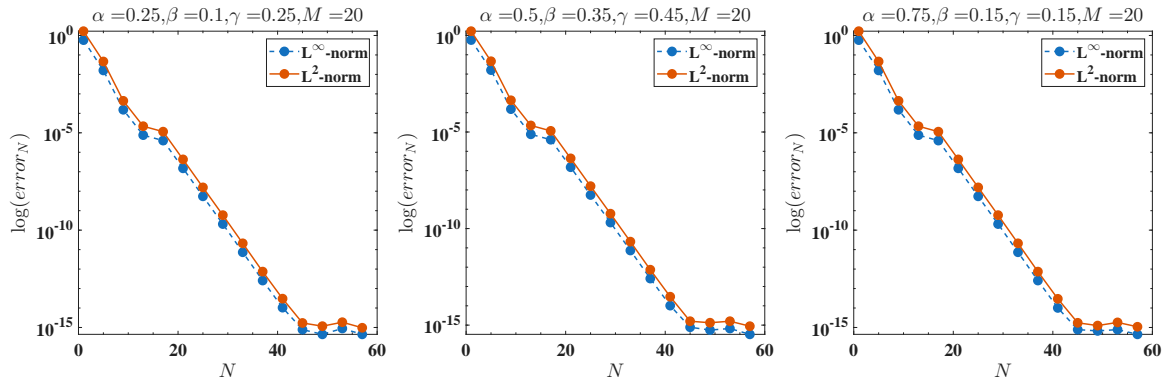


**Figure 5.3.** Exponential convergence of the CIM in time. Errors are shown for different fractional orders with an increasing number of quadrature points  $N$ , with given parameters  $M = 20$ ,  $a = 1$ ,  $b = 1000$ , and  $\kappa = 1/4$  (low temporal regularity).

**Table 1**

Spatial convergence order and  $\text{error}_M$  of the CIM-FLG for 1D inhomogeneous problem (Example 5.2) with  $\Lambda = 150$ ,  $t_0 = 0.01$ ,  $N = 50$ ,  $a = 10$ ,  $b = 10$ , and  $t = 0.5$ .

| M  | $\alpha = 0.25, \beta = 0.10, \gamma = 0.25$ |                |                   |                | $\alpha = 0.5, \beta = 0.35, \gamma = 0.45$ |                 |                   |                |
|----|--|----------------|-------------------|----------------|---|-----------------|-------------------|----------------|
|    | $L^2$ -error                                 | Order          | $L^\infty$ -error | Order          | $L^2$ -error                                | Order           | $L^\infty$ -error | Order          |
| 4  | 6.3122E-02                                   | —              | 4.4634E-02        | —              | 6.3123E-02                                  | —               | 4.4634E-02        | —              |
| 6  | 1.2349E-03                                   | $M^{-9.7027}$  | 7.2972E-04        | $M^{-10.1453}$ | 1.2349E-03                                  | $M^{-9.7026}$   | 7.2972E-04        | $M^{-10.1453}$ |
| 8  | 1.9993E-05                                   | $M^{-14.3331}$ | 9.9806E-06        | $M^{-14.9193}$ | 1.9993E-05                                  | $M^{-14.3331}$  | 9.9806E-06        | $M^{-14.9193}$ |
| 10 | 2.5826E-07                                   | $M^{-19.4903}$ | 1.1835E-07        | $M^{-19.8739}$ | 2.5826E-07                                  | $M^{-19.4903}$  | 1.1835E-07        | $M^{-19.8739}$ |
| 12 | 2.6230E-09                                   | $M^{-25.1735}$ | 1.0815E-19        | $M^{-25.7530}$ | 2.6230E-09                                  | $M^{-25.1735}$  | 1.0815E-09        | $M^{-25.7530}$ |
| 14 | 2.1245E-11                                   | $M^{-31.2416}$ | 8.2948E-12        | $M^{-31.5952}$ | 2.1245E-11                                  | $M^{-31.24170}$ | 8.2949E-12        | $M^{-31.5952}$ |
| 16 | 1.3955E-13                                   | $M^{-37.6352}$ | 5.0293E-14        | $M^{-38.2345}$ | 1.3957E-13                                  | $M^{-37.6339}$  | 5.0071E-14        | $M^{-38.2678}$ |

computational efficiency for the classical JE (with  $\alpha = \beta = \gamma = 1.0$ ). Moreover, Table 3 highlights the significant acceleration attained when the CIM-CLG algorithm is combined with FFT. Collectively, these numerical experiments confirm that the CIM-CLG algorithm devel-

**Table 2**

*Spatial convergence order and error<sub>M</sub> of the CIM-FLG for 1D inhomogeneous problem (Example 5.2) with  $\Lambda = 150$ ,  $t_0 = 0.01$ ,  $N = 50$ ,  $a = 10$ ,  $b = 10$ , and  $t = 0.5$ .*

| M  | $\alpha = 0.75, \beta = 0.15, \gamma = 0.15$ |                |                   |                | $\alpha = 1.0, \beta = 1.0, \gamma = 1.0$ |                |                   |                |
|----|--|----------------|-------------------|----------------|---|----------------|-------------------|----------------|
|    | $L^2$ -error                                 | Order          | $L^\infty$ -error | Order          | $L^2$ -error                              | Order          | $L^\infty$ -error | Order          |
| 4  | 6.3124E-02                                   | —              | 4.4635E-02        | —              | 6.3126E-02                                | —              | 4.4637E-02        | —              |
| 6  | 1.2349E-03                                   | $M^{-9.7027}$  | 7.2973E-04        | $M^{-10.1453}$ | 1.2349E-03                                | $M^{-9.7027}$  | 7.2975E-04        | $M^{-10.1454}$ |
| 8  | 1.9993E-05                                   | $M^{-14.3331}$ | 9.9806E-06        | $M^{-14.9193}$ | 1.9993E-05                                | $M^{-14.3331}$ | 9.9806E-06        | $M^{-14.9194}$ |
| 10 | 2.5826E-07                                   | $M^{-19.4903}$ | 1.1835E-07        | $M^{-19.8739}$ | 2.5826E-07                                | $M^{-19.4903}$ | 1.1835E-07        | $M^{-19.8739}$ |
| 12 | 2.6230E-09                                   | $M^{-25.1735}$ | 1.0815E-09        | $M^{-25.7531}$ | 2.6230E-09                                | $M^{-25.1735}$ | 1.0815E-09        | $M^{-25.7530}$ |
| 14 | 2.1245E-11                                   | $M^{-31.2416}$ | 8.2948E-12        | $M^{-31.5952}$ | 2.1245E-11                                | $M^{-31.2417}$ | 8.2949E-12        | $M^{-31.5952}$ |
| 16 | 1.3967E-13                                   | $M^{-37.6289}$ | 5.0182E-14        | $M^{-38.2511}$ | 1.3969E-13                                | $M^{-37.6274}$ | 5.0293E-14        | $M^{-38.2346}$ |

**Table 3**

*The CPU time cost and the needs of polynomial degree M in solving the inhomogeneous case of 1D problem (Example 5.2) by CIM-FLG with  $N = 50$ ,  $t = 0.5$  and prescript error  $\|p(t, r) - p_M^N\|_{L^2(\infty)} \leq 2.2025 \times 10^{-5}$ .*

|                     | $a = 1, b = 100, t = 0.5$ |                    | $a = 1, b = 100, t = 0.5$ |                    |
|---------------------|---------------------------|--------------------|---------------------------|--------------------|
|                     | (0.25, 0.10, 0.25)        | (0.50, 0.35, 0.45) | (0.75, 0.15, 0.15)        | (1.00, 1.00, 1.00) |
| Polynomial degree M | 14                        | 14                 | 14                        | 14                 |
| CPU time (s)        | 0.0937                    | 0.0944             | 0.0953                    | 0.0890             |

oped in this paper delivers robust numerical performance, including spatio-temporal spectral accuracy, and is effective for solving both the MT-TFJE and the classical JE.

**5.3. Example 3. (Homogeneous 1D problem).** This example examines the numerical performance of the proposed scheme applied to the homogeneous case of Problem (1.6). To illustrate the dynamic behaviors governed by both the MT-TFJE and its classical counterpart JE, we visualize the evolution of the numerical solution  $p(t, x)$  in one spatial dimension under varying parameters  $\alpha$ ,  $\beta$ , and  $\gamma$ . The problem is configured with zero source term ( $f \equiv 0$ ) and initial condition given by

- $p(0, x) = \exp(-30x^2)$ .

Since no analytical solution is available in this setting, we assess numerical accuracy through relative error measures. Specifically, Tables 4–6 report the  $L^2$ -error of the CIM temporal discretization, together with the spatial  $L^2$ -error,  $L^\infty$ -error, and corresponding convergence orders of the CLG scheme under different parameter configurations. A reference solution computed using  $N = 100$  quadrature points is adopted for error assessment. Additionally, Fig. 5.4 displays the evolution of the solution under various parameter values. These comprehensive numerical experiments confirm the reliability and high accuracy of the proposed scheme in simulating both MT-TFJE and classical JE.

**5.4. Example 4. (Homogeneous 2D problem).** In this example, we consider a two-dimensional homogeneous problem solved by the CIM-CLG algorithm, with the evolution of the numerical solution visualized. The system is subject to the initial condition

- $p_0(x, y) = -\pi^{-3}(0.75 + 0.3 \cos(\pi x))^{-1}(0.75 + 0.3 \sin(\pi y))^{-1}e^{-10xy}$ .

Numerical results under various parameter configurations are summarized in Tables 7–9,

**Table 4**

The errors  $\text{error}_N$  of CIM-FLG for 1D homogeneous problem (Example 5.3) with  $\Lambda = 150$ ,  $t_0 = 0.01$ ,  $a = 10$ ,  $b = 10$ ,  $M = 20$  and  $t = 0.5$ .

| $(\alpha, \beta, \gamma)$ | $N$ | 4          | 6          | 10         | 20         | 30         | 50         |
|---------------------------|-----|------------|------------|------------|------------|------------|------------|
| (0.25, 0.10, 0.25)        |     | 9.4000E-04 | 1.7688E-03 | 3.8173E-05 | 1.0396E-08 | 1.6637E-11 | 1.9752E-16 |
| (0.50, 0.35, 0.45)        |     | 2.8532E-03 | 1.9841E-03 | 4.4240E-05 | 1.5780E-08 | 2.1594E-11 | 1.6251E-16 |
| (0.75, 0.15, 0.15)        |     | 2.4563E-03 | 2.4607E-03 | 5.6212E-05 | 1.8726E-08 | 2.4277E-11 | 1.1142E-16 |
| (1.00, 1.00, 1.00)        |     | 9.1824E-03 | 1.2907E-03 | 8.4327E-05 | 2.0863E-08 | 2.8936E-11 | 3.1115E-16 |

**Table 5**

Spatial convergence order and  $\text{error}_M$  of CIM-FLG for 1D homogeneous problem (Example 5.3 with  $\Lambda = 150$ ,  $t_0 = 0.01$ ,  $a = 10$ ,  $b = 10$ ,  $N = 50$  and  $t = 0.5$ .

| $M$ | $\alpha = 0.25, \beta = 0.10, \gamma = 0.25$ |               |                   |               | $\alpha = 0.50, \beta = 0.35, \gamma = 0.45$ |               |                   |               |
|-----|--|---------------|-------------------|---------------|--|---------------|-------------------|---------------|
|     | $L^2$ -error                                 | Order         | $L^\infty$ -error | Order         | $L^2$ -error                                 | Order         | $L^\infty$ -error | Order         |
| 6   | 7.1487E-02                                   | —             | 4.9776E-02        | —             | 7.0297E-02                                   | —             | 4.8420E-02        | —             |
| 12  | 5.1394E-03                                   | $M^{-3.7980}$ | 2.2142E-03        | $M^{-4.4906}$ | 5.0474E-03                                   | $M^{-3.7998}$ | 2.0330E-03        | $M^{-4.5739}$ |
| 24  | 2.1303E-03                                   | $M^{-1.2706}$ | 5.9757E-04        | $M^{-1.8896}$ | 2.1151E-03                                   | $M^{-1.2548}$ | 6.0260E-04        | $M^{-1.7543}$ |

**Table 6**

Spatial convergence order and  $\text{error}_M$  of CIM-FLG for 1D homogeneous problem (Example 5.3) with  $\Lambda = 150$ ,  $t_0 = 0.01$ ,  $a = 10$ ,  $b = 10$ ,  $N = 50$  and  $t = 0.5$ .

| $M$ | $\alpha = 0.75, \beta = 0.15, \gamma = 0.15$ |               |                   |               | $\alpha = 1.00, \beta = 1.00, \gamma = 1.00$ |               |                   |               |
|-----|--|---------------|-------------------|---------------|--|---------------|-------------------|---------------|
|     | $L^2$ -error                                 | Order         | $L^\infty$ -error | Order         | $L^2$ -error                                 | Order         | $L^\infty$ -error | Order         |
| 6   | 6.8378E-02                                   | —             | 4.6514E-02        | —             | 7.4670E-02                                   | —             | 4.8411E-02        | —             |
| 12  | 4.9166E-03                                   | $M^{-3.7978}$ | 1.8325E-03        | $M^{-4.6658}$ | 5.4849E-03                                   | $M^{-3.7670}$ | 1.9798E-03        | $M^{-4.6119}$ |
| 24  | 2.0815E-03                                   | $M^{-1.2401}$ | 6.0649E-04        | $M^{-1.5953}$ | 2.3835E-03                                   | $M^{-1.2024}$ | 7.3515E-04        | $M^{-1.4293}$ |

**Table 7**

The errors  $\text{error}_N$  of CIM-FLG for 2D homogeneous problem (Example 5.4) with  $\Lambda = 150$ ,  $t_0 = 0.01$ ,  $a = 10$ ,  $b = 10$ ,  $M = 12$  and  $t = 0.5$ .

| $(\alpha, \beta, \gamma)$ | $N$ | 4          | 6          | 10         | 20         | 30         | 50         |
|---------------------------|-----|------------|------------|------------|------------|------------|------------|
| (0.25, 0.10, 0.25)        |     | 1.3895E-01 | 3.5169E-03 | 2.4167E-03 | 7.2364E-10 | 8.8657E-13 | 8.1332E-13 |
| (0.50, 0.35, 0.45)        |     | 5.5365E-02 | 6.1928E-03 | 1.4888E-03 | 4.4390E-10 | 9.7655E-13 | 7.2554E-13 |
| (0.75, 0.15, 0.15)        |     | 1.6974E-01 | 1.4018E-02 | 8.0089E-03 | 2.0357E-09 | 3.2825E-12 | 2.6205E-12 |
| (1.00, 1.00, 1.00)        |     | 1.9945E-01 | 6.0303E-02 | 1.3810E-02 | 5.8716E-09 | 2.8600E-12 | 2.7158E-12 |

and the temporal evolution for three representative cases is depicted in Fig. 5.5. This approach tightly integrates two objectives—validating the algorithm and understanding the features of the solution—highlighting its practical utility. Furthermore, it demonstrates the high numerical performance and robustness of our proposed algorithm in solving higher-dimensional problems.

**6. Concluding remarks.** In this work, we present a comprehensive study of the generalized Jeffreys-type law governed by a multi-term time-fractional Jeffreys-type equation (MT-TFJE), integrating stochastic modeling, regularity analysis, and high-accuracy numerical computation. The governing equation is derived from first principles via microscopic

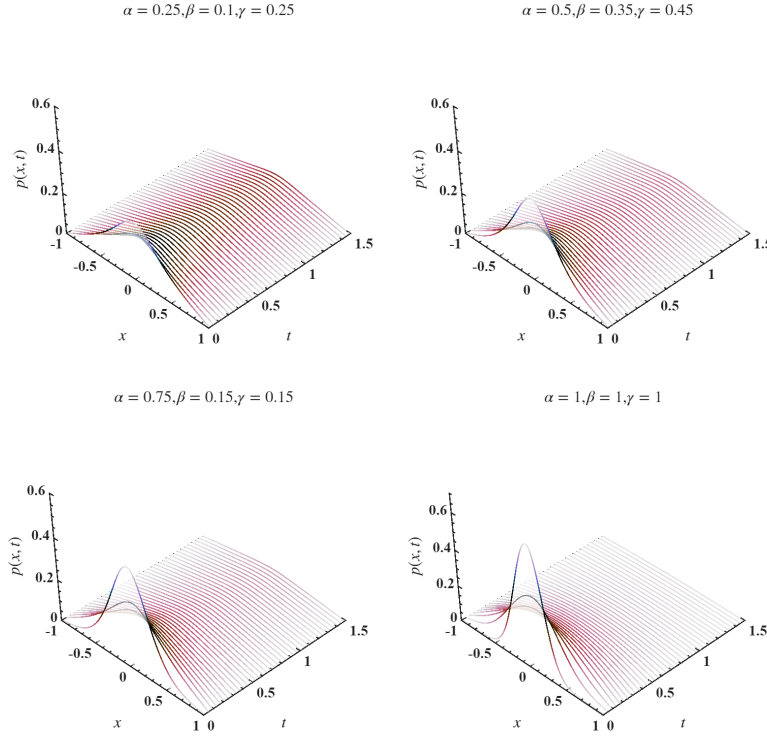


**Figure 5.4.** The dynamic behavior of the two-dimensional solution  $p(x, t)$  to 1-D Problem (1.6) under varying fractional orders are presented. The numerical experiment uses the following parameter values:  $\Lambda = 150$ ,  $t_0 = 0.01$ ,  $N = 50$ ,  $M = 128$ ,  $a = 10$ , and  $b = 10$ , with initial condition  $p_0(x) = \exp(-30x^2)$ , as specified in Example 5.3.

**Table 8**

Spatial convergence order and error of CIM-FLG for 2D homogeneous problem (Example 5.4) with  $\Lambda = 150$ ,  $t_0 = 0.01$ ,  $a = 10$ ,  $b = 10$ ,  $N = 50$  and  $t = 0.5$ .

| M  | $\alpha = 0.25, \beta = 0.15, \gamma = 0.25$ |               |                   |               | $\alpha = 0.50, \beta = 0.35, \gamma = 0.45$ |               |                   |               |
|----|--|---------------|-------------------|---------------|--|---------------|-------------------|---------------|
|    | $L^2$ -error                                 | Order         | $L^\infty$ -error | Order         | $L^2$ -error                                 | Order         | $L^\infty$ -error | Order         |
| 6  | 4.2408E-02                                   | —             | 2.9598E-02        | —             | 4.9963E-03                                   | —             | 3.4536E-03        | —             |
| 12 | 2.4301E-03                                   | $M^{-2.0626}$ | 1.3158E-03        | $M^{-2.2457}$ | 2.8469E-04                                   | $M^{-2.0667}$ | 1.4780E-04        | $M^{-2.2732}$ |
| 24 | 2.3139E-04                                   | $M^{-1.6963}$ | 6.4573E-05        | $M^{-2.1744}$ | 1.4283E-05                                   | $M^{-1.6853}$ | 7.8389E-06        | $M^{-2.1184}$ |

stochastic processes, including an extended continuous-time random walk model and an over-damped Langevin equation coupled with a time-changing process. This derivation establishes a physical foundation for the MT-TFJE and clarifies its capacity to describe crossover diffusion phenomena characterized by distinct scaling exponents. We further establish the well-posedness and Sobolev regularity of the model, providing a priori estimates under both smooth and non-smooth initial data while laying a foundation for subsequent numerical error analysis. A novel spectral-accurate numerical, termed the CIM-CLG algorithm, is developed by combining a contour integral method for time discretization with a Chebyshev-Legendre Galerkin

**Table 9**

*Spatial convergence order and error<sub>M</sub> of CIM-FLG for 2D homogeneous problem (Example 5.4) with  $\Lambda = 150$ ,  $t_0 = 0.01$ ,  $a = 10$ ,  $b = 10$ ,  $N = 50$  and  $t = 0.5$ .*

| M  | $\alpha = 0.75, \beta = 0.15, \gamma = 0.15$ |               |                   |               | $\alpha = 1.00, \beta = 1.00, \gamma = 1.00$ |               |                   |               |
|----|--|---------------|-------------------|---------------|--|---------------|-------------------|---------------|
|    | $L^2$ -error                                 | Order         | $L^\infty$ -error | Order         | $L^2$ -error                                 | Order         | $L^\infty$ -error | Order         |
| 6  | 5.9357E-03                                   | —             | 3.9014E-03        | —             | 2.0282E-02                                   | —             | 1.3753E-02        | —             |
| 12 | 3.3586E-04                                   | $M^{-2.0717}$ | 1.3929E-04        | $M^{-2.4039}$ | 1.1474E-03                                   | $M^{-2.0719}$ | 5.4455E-04        | $M^{-2.3292}$ |
| 24 | 3.4564E-05                                   | $M^{-1.6403}$ | 1.0591E-05        | $M^{-1.8586}$ | 1.1411E-04                                   | $M^{-1.6649}$ | 3.3661E-05        | $M^{-2.0080}$ |

scheme for spatial approximation. The proposed algorithm achieves spectral accuracy in both space and time with significantly reduced computational and storage costs, supports full parallelism, and accommodates low temporal regularity in the solution. Detailed implementation procedures and new technical error estimates are provided. Extensive numerical experiments in one and two dimensions confirm the efficiency, accuracy, and robustness of the scheme, validating the theoretical findings and illustrating the dynamic behavior of the underlying system.

The spatial semi-discrete CLG scheme requires specific geometric constraints on the computational domain, which limits its direct extension to problems defined on irregular regions. A practical workaround is to leverage the decay properties of the solution by embedding complex domains into larger regular domains, for example, circular or spherical regions, prior to numerical discretization. While effective, this domain-embedding strategy inevitably increases computational cost. Nevertheless, the high efficiency of the CIM maintains high accuracy even with a small number of quadrature points  $N$  (e.g.,  $N = 16$ ). For applications requiring faster computation, the acceleration strategy introduced in [43] can be incorporated into the current framework.

**Appendix A. Definitions.** The analysis of Prop. 2.1 relies on the properties of certain key functions, whose formal definitions and foundational properties we now recall.

**Definition A.1 (Bernstein functions, see, e.g., [5, 60]).**

**Completely monotone function** *The function  $\hat{u}(\xi) : (0, \infty) \rightarrow \mathbb{R}_+^0$  is a completely monotone (c.m.) function if it belongs to  $C^n(0, \infty)$  with respect to  $\xi$  and satisfies the condition  $(-1)^n \partial_\xi^n u(\xi) \geq 0$  for all  $n = 0, 1, 2, \dots$ ;*

**Stieltjes function** *The function  $\hat{u}(\xi) : (0, \infty) \rightarrow \mathbb{R}_+^0$  is a Stieltjes function (SF) with respect to  $\xi$  if there exists a c.m. function  $u(t)$  with respect to  $t > 0$  such that  $\hat{u}(\xi) = \int_0^\infty e^{-\xi t} u(t) dt$ ;*

**Bernstein function** *The function  $\hat{u}(\xi) : (0, \infty) \rightarrow \mathbb{R}_+^0$  is a Bernstein function (BF) if  $\hat{u}(\xi)$  is of class  $C^\infty$  and satisfies the condition  $(-1)^{n-1} \hat{u}^{(n)}(\xi) \geq 0$  for all  $n \in \mathbb{N}$ ;*

**Complete Bernstein function** *The Bernstein function  $\hat{u}(\xi) : (0, \infty) \rightarrow \mathbb{R}_+^0$  is said to be a complete Bernstein function (CBF), with respect to the same variable  $\xi$  if, and only if,  $\hat{u}(\xi)/\xi$  is a Stieltjes function.*

**Remark A.2.** Let  $\mathcal{CMF}$ ,  $\mathcal{SF}$ ,  $\mathcal{BF}$  and  $\mathcal{CBF}$  denote the sets of completely monotone functions, Stieltjes functions, Bernstein functions and complete Bernstein functions, respectively, as defined in Definatian A.1. The following properties hold (see, e.g., [5, 7, 8, 60]):

(i) A function  $\hat{u}(\xi) \in \mathcal{CMF}$  if and only if there exists a nonnegative function  $u(t) \geq 0$  such

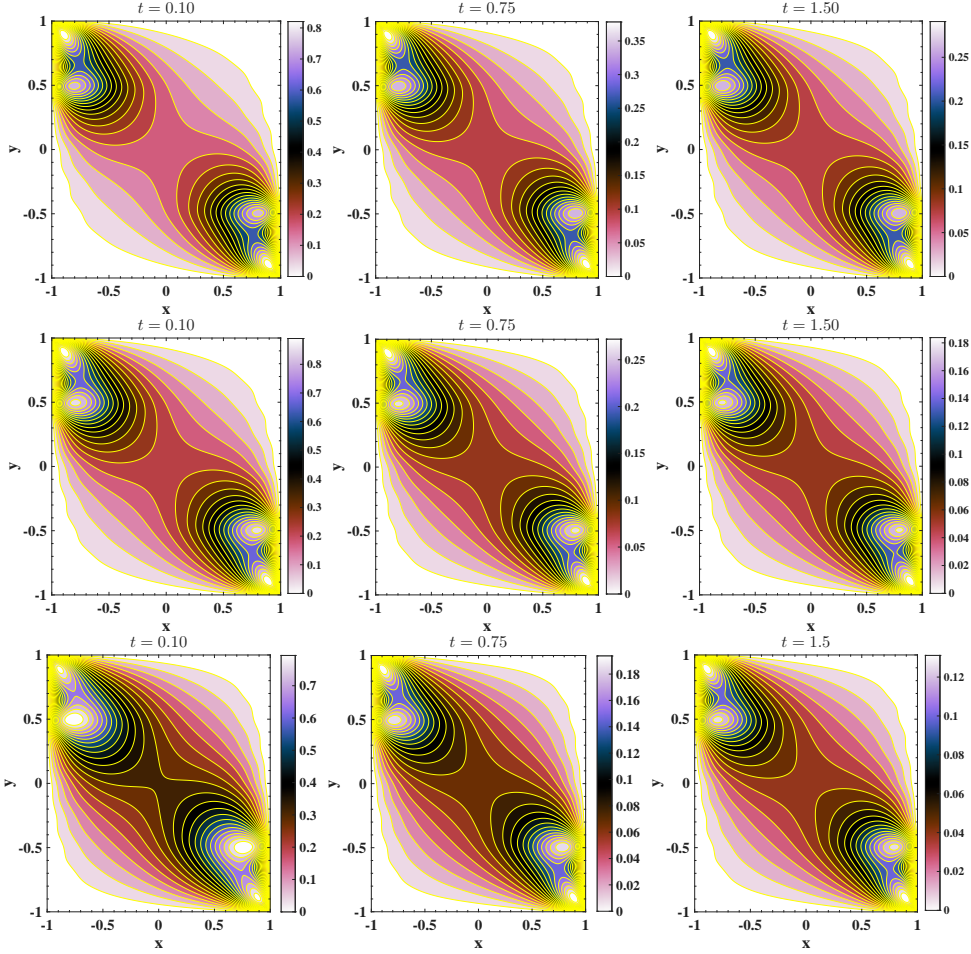


**Figure 5.5.** Dynamic behavior of the two-dimensional solution  $p(t, x, y)$  to Problem (1.6) for the initial condition in Example (5.4) with a vanishing source term. The top row depicts the case with fractional orders  $\alpha = 0.25$ ,  $\beta = 0.15$ ,  $\gamma = 0.25$ ; the middle row is the case with fractional orders  $\alpha = 0.50$ ,  $\beta = 0.35$ ,  $\gamma = 0.45$ ; while the bottom row corresponds to the classical case  $\alpha = 0.75$ ,  $\beta = 0.15$ ,  $\gamma = 0.15$ . Other parameters are fixed at  $M = 20$ ,  $a = 10$ ,  $b = 10$ ,  $\Lambda = 150$ , and  $t_0 = 0.01$ .

that  $\hat{u}(\xi) = \int_0^\infty u(t) \exp(-\xi t) dt$ ,  $\xi > 0$ . According to Bernstein's theorem [60, Thm.1.4], a function is c.m. if and only if it is the Laplace transform of a non-negative measure. Moreover, the product and nonnegative linear combination of two c.m. functions are also c.m..

(ii) Every SF is a c.m. function (i.e.,  $\mathcal{SF} \subset \mathcal{CMF}$ ), but the converse is not always true. The nonnegative linear combination of two Stieltjes functions is also a SF. However, the product of two Stieltjes functions does not always yield a SF. If  $\hat{u}, \hat{v} \in \mathcal{SF}$  with  $\alpha, \beta \in (0, 1)$  and  $\alpha + \beta \leq 1$ , then  $[\hat{u}(\xi)]^\alpha [\hat{v}(\xi)]^\beta \in \mathcal{SF}$ .

(iii) If  $\hat{u}, \hat{v} \in \mathcal{BF}$  and  $\hat{h} \in \mathcal{CMF}$ , then the compositions  $\hat{u}[\hat{v}(\xi)] \in \mathcal{BF}$ ,  $\hat{h}[\hat{u}(\xi)] \in \mathcal{CMF}$ , and  $\hat{u}(\xi)/\xi \in \mathcal{CMF}$ .

(iv) The nonnegative linear combination of CBFs is also a CBF. However, the product of two CBFs is not necessarily a CBF. If  $\hat{u}, \hat{v} \in \mathcal{CBF}$  and  $\alpha, \beta \in (0, 1)$  with  $\alpha + \beta \leq 1$ , then

$[\hat{u}(\xi)]^\alpha [\hat{v}(\xi)]^\beta \in \mathcal{CBF}$ . Furthermore, if  $\hat{u}(\xi) \in \mathcal{CBF}$ , then for any  $a, \xi > 0$ , the function  $\exp(-a\hat{u}(\xi)) \in \mathcal{CMF}$ .

Some useful scenarios described in Remark A.2 can be visualized in the following diagram:

$$\begin{array}{ccc}
 \mathcal{SF} & \xrightarrow{(\mathcal{SF} \subset \mathcal{CMF})} & \mathcal{CMF} \\
 \uparrow 1/\hat{u}(\xi) & \nearrow \exp(-a\hat{u}(\xi)), a>0 & \uparrow \hat{u}(\xi)/\xi \\
 \mathcal{CBF} & \xrightarrow{(\mathcal{CBF} \subset \mathcal{BF})} & \mathcal{BF}
 \end{array}$$

### Appendix B. The proof of Lemma 4.2.

*Proof.* Let  $z(\phi) \in \mathcal{N}_d \subseteq \Sigma_\theta$ . For  $|z| > \delta > 1$  and  $\alpha + \gamma < 1$ , it follows from Lemma 3.2 and the definition of  $\hat{p}(r, z)$  in (3.3) that

$$(B.1) \quad \|\hat{p}(r, z)\|_{L^2(\Omega)} \leq C(|z|^{-1}\|p_0\|_{L^2(\Omega)} + |z|^{-(\alpha+\gamma)}\|\hat{f}(z)\|_{(\mathcal{N}_d; L^2(\Omega))})$$

$$(B.2) \quad \leq C|z|^{-(\alpha+\gamma)}(\|p_0\|_{L^2(\Omega)} + \|\hat{f}(z)\|_{(\mathcal{N}_d; L^2(\Omega))}).$$

From (4.1), we have  $z'(\phi) = i\mu \cos(i\phi - \tilde{\alpha})$ . Let  $\phi = x + iy \in \mathcal{S}$  with  $0 < y < d$ . Then,

$$(B.3) \quad u(t, x + iy) = \frac{\mu}{2\pi} e^{\mu(1-\sin(\tilde{\alpha}+y-ix))t} \cos(\tilde{\alpha} + y - ix) \hat{u}(\mu(1 - \sin(\tilde{\alpha} + y - ix))).$$

Let  $l' := \tilde{\alpha} + y$ , so that  $l' \in (\tilde{\alpha}, \tilde{\alpha} + d) \subset (0, \pi/2 - \delta')$ . Taking the  $L^2$ -norm to both sides yields

$$(B.4) \quad \|u(t, r, x + iy)\|_{L^2(\Omega)} \leq \frac{\mu}{2\pi} e^{\mu t(1 - \sin(l' \cosh x))} \|\cos(l' - ix) \hat{u}(\mu(1 - \sin(l' - ix)))\|_{L^2(\Omega)}.$$

Using the earlier estimate (B.1) and the identity (B.4), we obtain

$$\begin{aligned}
 & \|\cos(l' - ix) \hat{u}(\mu(1 - \sin(l' - ix)))\|_{L^2(\Omega)} \\
 & \leq \frac{C|\cos(l' - ix)|}{|\mu(1 - \sin(l' - ix))|^{\alpha+\gamma}} (\|p_0\|_{L^2(\Omega)} + \|\hat{f}(z)\|_{(\mathcal{N}_d; L^2(\Omega))}).
 \end{aligned}$$

Note that

$$\frac{|\cos(l' - ix)|}{|1 - \sin(l' - ix)|} \leq \sqrt{\frac{1 + \sin l'}{1 - \sin l'}} := \mathcal{P}(l'),$$

and

$$\begin{aligned}
 \frac{|\cos(l' - ix)|}{|\mu(1 - \sin(l' - ix))|^{\alpha+\gamma}} &= \frac{1}{|\mu(1 - \sin(l' - ix))|^{\alpha+\gamma-1}} \frac{|\cos(l' - ix)|}{|\mu(1 - \sin(l' - ix))|} \\
 &\leq \frac{\mathcal{P}(l')}{\mu^{\alpha+\gamma}(\cosh x - \sin l')^{\alpha+\gamma-1}}.
 \end{aligned}$$

Since  $\sin \tilde{\alpha} < \sin l' = \sin(\tilde{\alpha} + d)$ , we conclude that

$$\begin{aligned}
 (B.5) \quad \|u(t, r, x + iy)\|_{L^2(\Omega)} &\leq C\Theta e^{-\mu t_0 \sin(\tilde{\alpha}) \cosh(x)} e^{\mu t_0 \Lambda} (\cosh(x) - \sin(l'))^{1-\alpha-\gamma} \\
 &\leq C\Theta e^{-\mu t_0 \sin(\tilde{\alpha}) \cosh(x)} (\cosh(x))^{1-\alpha-\gamma},
 \end{aligned}$$

where  $\Theta := \frac{\mu^{1-\alpha-\gamma} \mathcal{P}(\tilde{\alpha}+d)}{2\pi} (\|p_0\|_{L^2(\Omega)} + \|\widehat{f}(z)\|_{(\mathcal{N}_d; L^2(\Omega))})$ .

A similar argument applies to the lower part of  $\mathcal{S}$ . For  $\phi = x - iy \in \mathcal{S}$  with  $-d < -y \leq 0$ , and  $\sin(\tilde{\alpha} - d) < \sin \tilde{\alpha} < \sin(\tilde{\alpha} + d)$ , we obtain

$$(B.6) \quad \|u(t, r, x - iy)\|_{L^2(\Omega)} \leq C\Theta e^{\mu t_0 \Lambda} e^{-\mu t_0 \sin(\tilde{\alpha}-d) \cosh(x)} (\cosh(x))^{1-\alpha-\gamma}.$$

Therefore, for any  $\phi = x \pm iy \in \mathcal{S}$ , the aforementioned estimates imply

$$\|u(t, r, \phi)\|_{L^2(\Omega)} \leq C\Theta e^{\mu t_0 \Lambda} e^{-\mu t_0 \sin(\tilde{\alpha}-d) \cosh(x)} (\cosh(x))^{1-\alpha-\gamma}.$$

Let  $\rho := 1 - \alpha - \gamma \in (0, 1)$  and  $\vartheta := \mu t_0 \sin(\tilde{\alpha} - d) > 0$ . For any  $\nu \in (0, 1)$ , following [38], we have

$$\begin{aligned} \|u(t, r, \phi)\|_{L^2(\Omega)} &\leq C\Theta \mu^{-\rho} e^{\mu t_0 \Lambda} \mu^\rho (\cosh x)^\rho e^{-\nu \vartheta \cosh x} e^{-(1-\nu)\vartheta \cosh x} \\ &\leq C\Theta \mu^{-\rho} \frac{e^{\mu t_0 \Lambda}}{t_0^\rho} \left( \frac{\rho}{\nu \sin(\tilde{\alpha} - d) e^{\nu \vartheta / \rho}} \right)^\rho e^{-(1-\nu)\vartheta \cosh x}, \end{aligned}$$

To justify the last inequality, observe that

$$\begin{aligned} \lim_{|x| \rightarrow \infty} \mu^\rho (\cosh x)^\rho e^{-\nu \vartheta \cosh x} &= \lim_{|x| \rightarrow \infty} \mu^\rho \left( \frac{\cosh x}{e^{\nu \vartheta \cosh x / \rho}} \right)^\rho = \lim_{|x| \rightarrow \infty} \mu^\rho \left( \frac{\rho (\cosh x)'}{\nu \vartheta (\cosh x)' e^{\nu \vartheta \cosh x / \rho}} \right)^\rho \\ (1/e^{\nu \vartheta \cosh x / \rho} = 1/e^{\nu \vartheta / \rho}, \text{ with } \nu \vartheta / \rho > 0, |x| \rightarrow \infty) \\ &= \frac{1}{t_0^\rho} \left( \frac{\rho}{\nu \sin(\tilde{\alpha} - d) e^{\nu \vartheta / \rho}} \right)^\rho. \end{aligned}$$

Define  $Q := \frac{1}{2\pi} \left( \frac{\rho}{\nu \sin(\tilde{\alpha} - d) e^{\nu \vartheta / \rho}} \right)^\rho \mathcal{P}(\tilde{\alpha} + d)$ . Combining all estimates completes the proof of lemma 4.2.  $\blacksquare$

**Acknowledgments.** The author expresses sincere gratitude to Prof. Weihua Deng for his invaluable academic guidance. Special thanks are extended to Prof. Heping Ma for generously providing the code for the two-dimensional Legendre-Chebyshev transform. The author is particularly indebted to Prof. Tiejun Li for his generous support and for offering precious opportunities for professional development.

## REFERENCES

- [1] R. A. ADAMS AND J. J. F. FOURNIER, *Sobolev Spaces*, vol. 140 of Pure and Applied Mathematics (Amsterdam), Elsevier/Academic Press, Amsterdam, second ed., 2003.
- [2] W. E. ALLEY AND B. J. ALDER, *Modification of Fick's law*, Phys. Rev. Lett., 43 (1979), pp. 653–656, <https://doi.org/10.1103/physrevlett.43.653>.
- [3] D. APPLEBAUM, *Lévy Processes And Stochastic Calculus*, vol. 116 of Cambridge Studies in Advanced Mathematics, Cambridge University Press, Cambridge, second ed., 2009, <https://doi.org/10.1017/CBO9780511809781>.
- [4] W. ARENDT, C. J. K. BATTY, M. HIEBER, AND F. NEUBRANDER, *Vector-Valued Laplace Transforms And Cauchy Problems*, vol. 96 of Monographs in Mathematics, Birkhäuser/Springer Basel AG, Basel, second ed., 2011, <https://doi.org/10.1007/978-3-0348-0087-7>.
- [5] E. AWAD, *Dual-phase-lag in the balance: Sufficiency bounds for the class of Jeffreys' equations to furnish physical solutions*, Int. J. Heat Mass Transf., 158 (2020), p. 119742, <https://doi.org/10.1016/j.ijheatmasstransfer.2020.119742>.

[6] E. AWAD AND R. METZLER, *Crossover dynamics from superdiffusion to subdiffusion: models and solutions*, Fract. Calc. Appl. Anal., 23 (2020), pp. 55–102, <https://doi.org/10.1515/fca-2020-0003>.

[7] E. AWAD, T. SANDEV, R. METZLER, AND A. CHECHKIN, *From continuous-time random walks to the fractional Jeffreys equation: Solution and properties*, Int. J. Heat Mass Transf., 181 (2021), p. 121839, <https://doi.org/10.1016/j.ijheatmasstransfer.2021.121839>.

[8] E. BAZHLEKOVA, *Subordination results for a class of multi-term fractional Jeffreys-type equations*, Fract. Calc. Appl. Anal., 27 (2024), pp. 1048–1072, <https://doi.org/10.1007/s13540-024-00275-3>.

[9] G. BEL AND E. BARKAI, *Weak ergodicity breaking in the continuous-time random walk*, Phys. Rev. Lett., 94 (2005), <https://doi.org/10.1103/physrevlett.94.240602>.

[10] J. P. BOUCHAUD AND A. GEORGES, *Anomalous diffusion in disordered media: Statistical mechanisms, models and physical applications*, Phys. Rep., 195 (1990), pp. 127–293, [https://doi.org/10.1016/0370-1573\(90\)90099-N](https://doi.org/10.1016/0370-1573(90)90099-N).

[11] P. C. BRESSLOFF AND J. M. NEWBY, *Stochastic models of intracellular transport*, Rev. Mod. Phys., 85 (2013), pp. 135—196, <https://doi.org/10.1103/revmodphys.85.135>.

[12] D. BROGIOLI AND A. VAILATI, *Diffusive mass transfer by nonequilibrium fluctuations: Fick's law revisited*, Phys. Rev. E, 63 (2000), p. 012105, <https://doi.org/10.1103/physreve.63.012105>.

[13] F. CHEN, Q. XU, AND J. S. HESTHAVEN, *A multi-domain spectral method for time-fractional differential equations*, J. Comput. Phys., 293 (2015), pp. 157–172, <https://doi.org/10.1016/j.jcp.2014.10.016>.

[14] M. J. COLBROOK, *Computing semigroups with error control*, SIAM J. Numer. Anal., 60 (2022), pp. 396–422, <https://doi.org/10.1137/21M1398616>.

[15] M. J. COLBROOK AND L. J. AYTON, *A contour method for time-fractional PDEs and an application to fractional viscoelastic beam equations*, J. Comput. Phys., 454 (2022), p. 110995, <https://doi.org/10.1016/j.jcp.2022.110995>.

[16] A. T. CONLISK, *Essentials Of Micro-And Nanofluidics: With Applications To The Biological And Chemical Sciences*, Cambridge University Press, 2012.

[17] E. CUESTA, C. LUBICH, AND C. PALENCIA, *Convolution quadrature time discretization of fractional diffusion-wave equations*, Math. Comp., 75 (2006), pp. 673–696, <https://doi.org/10.1090/S0025-5718-06-01788-1>.

[18] E. L. CUSSLER, *Diffusion: Mass Transfer In Fluid Systems*, Cambridge university press, 2009.

[19] W. DENG, R. HOU, W. WANG, AND P. XU, *Modeling Anomalous Diffusion: From Statistics To Mathematics*, World Scientific Publishing Co. Pte. Ltd., Hackensack, NJ, 2020.

[20] W. DENG, B. LI, Z. QIAN, AND H. WANG, *Time discretization of a tempered fractional Feynman-Kac equation with measure data*, SIAM J. Numer. Anal., 56 (2018), pp. 3249–3275, <https://doi.org/10.1137/17M1118245>.

[21] W. DENG AND Z. ZHANG, *High Accuracy Algorithm For The Differential Equations Governing Anomalous Diffusion*, World Scientific Publishing Co. Pte. Ltd., Hackensack, NJ, 2019.

[22] W. FELLER, *An Introduction To Probability Theory And Its Applications. Vol. II*, John Wiley & Sons, Inc., New York-London-Sydney, second ed., 1971.

[23] L. FENG, F. LIU, I. TURNER, AND L. ZHENG, *Novel numerical analysis of multi-term time fractional viscoelastic non-newtonian fluid models for simulating unsteady MHD Couette flow of a generalized Oldroyd-B fluid*, Fract. Calc. Appl. Anal., 21 (2018), pp. 1073–1103, <https://doi.org/10.1515/fca-2018-0058>.

[24] A. FICK, *Poggendorff's flannel*, Annalen der Physik, 94 (1855), p. 297.

[25] A. FICK, *Ueber diffusion*, Ann. Phys-Berlin, 170 (1855), pp. 59–86, <https://doi.org/10.1002/andp.18551700105>.

[26] H. C. FOGEDBY, *Langevin equations for continuous time Lévy flights*, Phys. Rev. E, 50 (1994), pp. 1657–1660, <https://doi.org/10.1103/physreve.50.1657>.

[27] P. L. GARRIDO, P. I. HURTADO, AND B. NADROWSKI, *Simple one-dimensional model of heat conduction which obeys Fourier's law*, Phys. Rev. Lett., 86 (2001), pp. 5486–5489, <https://doi.org/10.1103/physrevlett.86.5486>.

[28] B. JIN, *Fractional differential equations—an approach via fractional derivatives*, vol. 206 of Applied Mathematical Sciences, Springer, Cham, 2021, <https://doi.org/10.1007/978-3-030-76043-4>.

[29] B. JIN, R. LAZAROV, Y. LIU, AND Z. ZHOU, *The Galerkin finite element method for a multi-term time-fractional diffusion equation*, J. Comput. Phys., 281 (2015), pp. 825–843, <https://doi.org/10.1016/j.jcp.2014.09.031>.

jcp.2014.10.051.

[30] D. D. JOSEPH AND L. PREZIOSI, *Heat waves*, Rev. Modern Phys., 61 (1989), pp. 41–73, <https://doi.org/10.1103/RevModPhys.61.41>.

[31] J. KLAFTER AND I. M. SOKOLOV, *First steps in random walks*, Oxford University Press, Oxford, 2015. From tools to applications.

[32] F. LE VOT, E. ABAD, AND S. B. YUSTE, *Continuous-time random-walk model for anomalous diffusion in expanding media*, Phys. Rev. E, 96 (2017), p. 032117, <https://doi.org/10.1103/physreve.96.032117>.

[33] M. H. LEE, *Fick’s law, Green-Kubo formula, and Heisenberg’s equation of motion*, Phys. Rev. Lett., 85 (2000), pp. 2422–2425, <https://doi.org/10.1103/physrevlett.85.2422>.

[34] B. LI, Y. LIN, S. MA, AND Q. RAO, *An exponential spectral method using VP means for semilinear subdiffusion equations with rough data*, SIAM J. Numer. Anal., 61 (2023), pp. 2305–2326, <https://doi.org/10.1137/22M1512041>.

[35] B. LI AND S. MA, *A high-order exponential integrator for nonlinear parabolic equations with nonsmooth initial data*, J. Sci. Comput., 87 (2021), p. 23, <https://doi.org/10.1007/s10915-021-01438-7>.

[36] X. LI AND C. XU, *A space-time spectral method for the time fractional diffusion equation*, SIAM J. Numer. Anal., 47 (2009), pp. 2108–2131, <https://doi.org/10.1137/080718942>.

[37] J. LLOYD, T. RAKOVSKY, F. POLLMANN, AND C. VON KEYSERLINGK, *Ballistic to diffusive crossover in a weakly interacting fermi gas*, Phys. Rev. B, 109 (2024), <https://doi.org/10.1103/physrevb.109.205108>.

[38] M. LÓPEZ-FERNÁNDEZ AND C. PALENCIA, *On the numerical inversion of the Laplace transform of certain holomorphic mappings*, Appl. Numer. Math., 51 (2004), pp. 289–303, <https://doi.org/10.1016/j.apnum.2004.06.015>.

[39] M. LÓPEZ-FERNÁNDEZ, C. PALENCIA, AND A. SCHÄDLE, *A spectral order method for inverting sectorial Laplace transforms*, SIAM J. Numer. Anal., 44 (2006), pp. 1332–1350, <https://doi.org/10.1137/050629653>.

[40] C. LUBICH, I. H. SLOAN, AND V. THOMÉE, *Nonsmooth data error estimates for approximations of an evolution equation with a positive-type memory term*, Math. Comp., 65 (1996), pp. 1–17, <https://doi.org/10.1090/S0025-5718-96-00677-1>.

[41] Y. LUCHKO, *Initial-boundary-value problems for the generalized multi-term time-fractional diffusion equation*, J. Math. Anal. Appl., 374 (2011), pp. 538–548, <https://doi.org/10.1016/j.jmaa.2010.08.048>.

[42] F. MA, W. TIAN, AND W. DENG, *Mathematical modeling and analysis for the chemotactic diffusion in porous media with incompressible Navier-Stokes equations over bounded domain*, J. Differ. Equ., 436 (2025), p. 113305, <https://doi.org/10.1016/j.jde.2025.113305>.

[43] F. MA, L. ZHAO, W. DENG, AND Y. WANG, *Analyses of the contour integral method for time fractional normal-subdiffusion transport equation*, J. Sci. Comput., 97 (2023), p. 45, <https://doi.org/10.1007/s10915-023-02359-3>.

[44] F. MA, L. ZHAO, Y. WANG, AND W. DENG, *The contour integral method for Feynman-Kac equation with two internal states*, Comput. Math. Appl., 151 (2023), pp. 80–100, <https://doi.org/10.1016/j.camwa.2023.09.037>.

[45] H. MA, *Chebyshev-Legendre spectral viscosity method for nonlinear conservation laws*, SIAM J. Numer. Anal., 35 (1998), pp. 869–892, <https://doi.org/10.1137/S0036142995293900>.

[46] H. MA, *Chebyshev-Legendre super spectral viscosity method for nonlinear conservation laws*, SIAM J. Numer. Anal., 35 (1998), pp. 893–908, <https://doi.org/10.1137/S0036142995293912>.

[47] F. MAES AND K. VAN BOCKSTAL, *Existence and uniqueness of a weak solution to fractional single-phase-lag heat equation*, Fract. Calc. Appl. Anal., 26 (2023), pp. 1663–1690, <https://doi.org/10.1007/s13540-023-00177-w>.

[48] J. MASOLIVER, *Fractional telegrapher’s equation from fractional persistent random walks*, Phys. Rev. E, 93 (2016), pp. 052107, 10, <https://doi.org/10.1103/physreve.93.052107>.

[49] W. MCLEAN AND V. THOMÉE, *Time discretization of an evolution equation via Laplace transforms*, IMA J. Numer. Anal., 24 (2004), pp. 439–463, <https://doi.org/10.1093/imanum/24.3.439>.

[50] W. MCLEAN AND V. THOMÉE, *Maximum-norm error analysis of a numerical solution via Laplace transformation and quadrature of a fractional-order evolution equation*, IMA J. Numer. Anal., 30 (2010), pp. 208–230, <https://doi.org/10.1093/imanum/drp004>.

[51] M. M. MEERSCHAERT AND P. STRAKA, *Inverse stable subordinators*, Math. Model. Nat. Phenom., 8 (2013), pp. 1–16, <https://doi.org/10.1051/mmnp/20138201>.

[52] R. METZLER AND J. KLAFTER, *The random walk's guide to anomalous diffusion: A fractional dynamics approach*, Phys. Rep., 339 (2000), p. 77, [https://doi.org/10.1016/S0370-1573\(00\)00070-3](https://doi.org/10.1016/S0370-1573(00)00070-3).

[53] E. W. MONTROLL AND G. H. WEISS, *Random walks on lattices. II*, J. Mathematical Phys., 6 (1965), pp. 167–181, <https://doi.org/10.1063/1.1704269>.

[54] S. MUKHERJEE, R. K. SINGH, M. JAMES, AND S. S. RAY, *Anomalous diffusion and Lévy walks distinguish active from inertial turbulence*, Phys. Rev. Lett., 127 (2021), <https://doi.org/10.1103/physrevlett.127.118001>.

[55] K. MUSTAPHA, *An L1 approximation for a fractional reaction-diffusion equation, a second-order error analysis over time-graded meshes*, SIAM J. Numer. Anal., 58 (2020), pp. 1319–1338, <https://doi.org/10.1137/19M1260475>.

[56] R. PASTORE, A. CIARLO, G. PESCE, F. GRECO, AND A. SASSO, *Rapid Fickian yet non-Gaussian diffusion after subdiffusion*, Phys. Rev. Lett., 126 (2021), <https://doi.org/10.1103/physrevlett.126.158003>.

[57] S. A. RUKOLAIN AND A. M. SAMSONOV, *Local immobilization of particles in mass transfer described by a Jeffreys-type equation*, Phys. Rev. E, 88 (2013), p. 062116, <https://doi.org/10.1103/physreve.88.062116>.

[58] S. R. K. M. V. SANDEV, T. AND L. KOCAREV, *First-passage times for generalized heterogeneous telegrapher's processes*, Phys. Rev. E, 111 (2025), p. 044105, <https://doi.org/10.1103/PhysRevE.111.044105>.

[59] T. SANDEV, R. METZLER, AND A. CHECHKIN, *From continuous time random walks to the generalized diffusion equation*, Fract. Calc. Appl. Anal., 21 (2018), pp. 10–28, <https://doi.org/10.1515/fca-2018-0002>.

[60] R. S. SCHILLING, RENÉ L. AND Z. VONDRAČE, *Bernstein functions: Theory and applications*, Monographs in Mathematics, Walter de Gruyter, 2009.

[61] J. SHEN, *Efficient spectral-Galerkin method. I. Direct solvers of second- and fourth-order equations using Legendre polynomials*, SIAM J. Sci. Comput., 15 (1994), pp. 1489–1505, <https://doi.org/10.1137/0915089>.

[62] J. SHEN, *Efficient Chebyshev-Legendre Galerkin methods for elliptic problems*, in Proceedings of ICOSA-HOM, vol. 95, Citeseer, 1996, pp. 233–239.

[63] J. SHEN, T. TANG, AND L.-L. WANG, *Spectral Methods: Algorithms, Analysis And Applications*, vol. 41, Springer Science & Business Media, 2011.

[64] C.-S. SIN, J.-U. RIM, AND H.-S. CHOE, *Initial-boundary value problems for multi-term time-fractional wave equations*, Fract. Calc. Appl. Anal., 25 (2022), pp. 1994–2019, <https://doi.org/10.1007/s13540-022-00080-w>.

[65] I. M. SOKOLOV, *Models of anomalous diffusion in crowded environments*, Soft Matter, 8 (2012), p. 9043, <https://doi.org/10.1039/c2sm25701g>.

[66] H. SRINIVASAN, V. K. SHARMA, V. GARCÍA SAKAI, AND S. MITRA, *Nature of subdiffusion crossover in molecular and polymeric glassformers*, Phys. Rev. Lett., 132 (2024), <https://doi.org/10.1103/physrevlett.132.058202>.

[67] A. TALBOT, *The accurate numerical inversion of Laplace transforms*, IMA J. Appl. Math., 23 (1979), pp. 97–120, <https://doi.org/10.1093/imamat/23.1.97>.

[68] P. TAN, Y. LIANG, Q. XU, E. MAMONTOV, J. LI, X. XING, AND L. HONG, *Gradual crossover from subdiffusion to normal diffusion: A many-body effect in protein surface water*, Phys. Rev. Lett., 120 (2018), <https://doi.org/10.1103/physrevlett.120.248101>.

[69] J. A. C. WEIDEMAN AND L. N. TREFETHEN, *Parabolic and hyperbolic contours for computing the Bromwich integral*, Math. Comp., 76 (2007), pp. 1341–1356, <https://doi.org/10.1090/S0025-5718-07-01945-X>.

[70] H. WU, H. MA, AND H. LI, *Optimal error estimates of the Chebyshev-Legendre spectral method for solving the generalized Burgers equation*, SIAM J. Numer. Anal., 41 (2003), pp. 659–672, <https://doi.org/10.1137/S0036142901399781>.

[71] T. ZHAO, Y. WU, AND H. MA, *Error analysis of Chebyshev-Legendre pseudo-spectral method for a class of nonclassical parabolic equation*, J. Sci. Comput., 52 (2012), pp. 588–602, <https://doi.org/10.1007/s10915-011-9560-9>.